Phase diagram and continuous pair-unbinding transition of the bilinear-biquadratic $S = 1$ Heisenberg chain in a magnetic field

Salvatore R. Manmana,[1,*] Andreas M. Läuchli,[2] Fabian H. L. Essler,[3] and Frédéric Mila[1]
[1]*Institut de Théorie des Phénomènes Physiques, EPF Lausanne, CH-1015 Lausanne, Switzerland*
[2]*Max-Planck Institut für Physik Komplexer Systeme, Nöthnitzer Straße 38, D-01187 Dresden, Germany*
[3]*The Rudolf Peierls Centre for Theoretical Physics, Oxford University, Oxford OX1 3NP, United Kingdom*
(Received 20 December 2010; revised manuscript received 23 March 2011; published 31 May 2011)

We investigate the properties of the Heisenberg $S = 1$ chain with bilinear and biquadratic interactions in a magnetic field using the density- matrix renormalization-group, Bethe ansatz, and field-theoretical considerations. In a large region of the parameter space, we identify a magnetized ferroquadrupolar Luttinger liquid consisting of a quasicondensate of bound magnon pairs. This liquid undergoes a continuous pair-unbinding transition to a more conventional Luttinger liquid region obtained by polarizing the system above the Haldane gap region. This pair-unbinding transition is shown to be in the Ising universality class on top of a Luttinger liquid, leading to an effective central charge $3/2$. We also revisit the nature of the partially polarized Luttinger liquid around and above the Uimin-Lai-Sutherland point. Our results confirm that this is a two-component liquid and rule out the formation of a single-component vector-chiral phase.

DOI: 10.1103/PhysRevB.83.184433 PACS number(s): 75.10.Jm, 75.10.Pq, 75.40.Mg, 75.30.Kz

I. INTRODUCTION

A particularly interesting aspect of quantum many-body systems is their ability to host ordered phases that emerge from the spontaneous breaking of one or several of the symmetries of the system. In the case of spin systems, the main focus lies on possible long-range-order (LRO) due to the breaking of the SU(2) symmetry inherent to these systems. For $S = 1/2$ Heisenberg systems, breaking this continuous symmetry with a purely local order parameter implies magnetic ordering. However, when the spin is $S > 1/2$, there is the alternative possibility that the SU(2) symmetry is broken by a local quadrupolar order parameter, leading to spin-nematic phases.[1,2] Recent findings on $NiGa_2S_4$, a spin-1 material on a triangular lattice,[3] indicate the possible realization of such a spin-nematic phase. Theoretical investigations of the bilinear-biquadratic $S = 1$ Heisenberg model on this lattice geometry have shown that it is possible to stabilize spin-nematic LRO of ferroquadrupolar and antiferroquadrupolar type depending on the sign of the biquadratic interaction,[4,5] and that applying an external magnetic field leads to a remarkably rich phase diagram with, in particular, a $2/3$ magnetization plateau above the antiferroquadrupolar phase.[4]

In this paper we investigate the one-dimensional version of the model defined by the Hamiltonian

$$\mathcal{H} = J \sum_i [\cos\theta\, \mathbf{S}_i \cdot \mathbf{S}_{i+1} + \sin\theta\, (\mathbf{S}_i \cdot \mathbf{S}_{i+1})^2] - H S^z_{\mathrm{tot}}, \tag{1}$$

where $J, H > 0$. While a variety of materials realizing $S = 1$ Heisenberg systems are known,[6] the biquadratic term seems to be more difficult to realize in nature.[7] However, recent progress in the realization of effective spin Hamiltonians in systems of ultracold atomic gases on optical lattices[8–10] opens up a promising alternative route to investigate such systems in experiments.

At zero field, the properties of this model are well understood by now.[11–24] For our considerations, it is helpful to keep in mind the following aspects of its phase diagram. Between the two integrable points $\theta_{\mathrm{TB}} = -\pi/4$ (the Takhtajan-Babujian point,[14,15] TB) and $\theta_{\mathrm{ULS}} = \pi/4$ (the Uimin-Lai-Sutherland point,[11–13] ULS) the chain possesses a finite Haldane gap.[25,26] In this phase, at the so-called AKLT point (named after Affleck, Kennedy, Lieb, and Tasaki, Ref. 16) $\theta_{\mathrm{AKLT}} = \arctan 1/3$, the ground state is exactly known to be a valence bond solid, and for $\theta > \theta_{\mathrm{AKLT}}$ the spin-correlation functions become incommensurate.[22,27] Between the ULS point and $\theta = \pi/2$, the system is gapless and shows antiferroquadrupolar spin-nematic quasi-long-range order (QLRO).[24] For negative values of θ, between $\theta = -3/4\pi$ and $\theta = -\pi/4$, the system is dimerized and has a finite gap.[17–19,23] For the remaining values of θ, the system is in a ferromagnetic state.

In comparison, the properties in a field have been investigated less intensively. Most of the attention has been devoted to the region of positive and not too large biquadratic interaction,[28–31] and large regions of the phase diagram remain unexplored. For instance, the fate of the spin-nematic phase, realized at zero field in the region $\pi/4 < \theta < \pi/2$,[24] remains an open issue, and the finite field properties of the model for negative biquadratic interactions are largely unexplored, including the finite field properties of the integrable TB point.

In this paper, we complete previous studies and consider the *full* phase diagram at finite magnetic fields over the whole range of θ by applying the density-matrix renormalization-group method (DMRG),[32,33] complemented by a Bethe ansatz (BA) solution of the TB and ULS points in magnetic-field and field-theoretical considerations. We put special emphasis on the possible realization of spin-nematic QLRO in the presence of a field by explicitly computing the spin-nematic correlation functions in real space.

The scope of this paper is fourfold. First, by considering the full phase diagram of the system at finite magnetic fields we want to make precise predictions for ongoing efforts in the realization of such models in systems of ultracold atomic gases on optical lattices and for future quantum magnetic materials, which eventually may be described in terms of

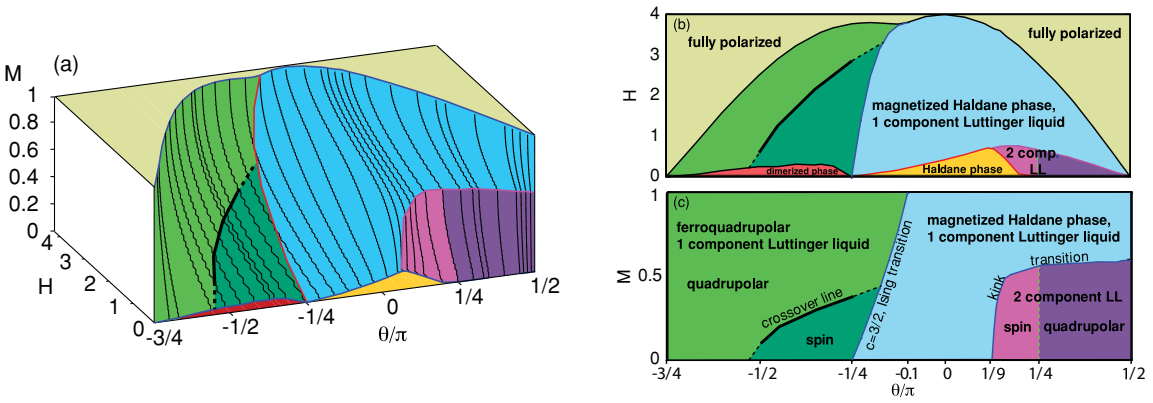

FIG. 1. (Color online) (a) DMRG results for systems with $L = 60$ lattice sites for the magnetization of the BLBQ $S = 1$ chain as a function of (H,θ). The various colors indicate the different phases of the system. (b) Phase diagram obtained from the DMRG results for the magnetization, the correlation functions defined in Eqs. (3)–(5) and (10), and for the central charge c as a function of (H,θ), and (c) as a function of (M,θ). The black line in the magnetized dimer phase indicates a crossover line at which the exponents of C_S^{long} and $C_{Q,2}$ are both equal to 1; see Sec. III C 4 (the dashed lines are linear extrapolations to the boundary of the phase and serve as a guide to the eye). The green dashed line below the kink transition indicates a crossover line between two different two-channel LL phases, one of them being a spin-nematic LL. Note that, as discussed in Sec. III D 2, this line is not exactly at $\theta = \pi/4$ but seems to wind around this value.

the bilinear-biquadratic (BLBQ) chain. Second, we address the possibility to realize unconventional QLRO by explicitly computing the spin-nematic correlation functions in real space. Third, we consider in detail the phase transitions at finite field and study their critical behavior. Fourth, we address the possibility to realize vector-chiral LRO as identified previously in frustrated $S = 1/2$ chains in a magnetic field, which has been proposed for the BLBQ chain in a magnetic field.[34] We will demonstrate that the magnetic field leads to the realization of five different Luttinger liquid (LL) phases, and that these magnetic phases are connected to each other by either continuous phase transitions or crossovers. Our findings are summarized in Fig. 1, which shows our DMRG results for the magnetization as a function of (H,θ) and the main result of this paper, which is the complete phase diagram of the BLBQ chain in a magnetic field.

The paper is organized as follows. In Sec. II we introduce the observables relevant for the description of the various LL phases. In Sec. III we present the complete phase diagram as a function of (H,θ) by discussing our results for the magnetization (Sec. III A), for the central charge (Sec. III B), for the correlation functions in the single-component LL phases (Sec. III C), and for the correlation functions in the two-component LL phases (Sec. III D). Concerning the single-component LL phases, we demonstrate in Sec. III C 3 that a ferroquadrupolar LL phase is realized, and we discuss the extension of the magnetized Haldane phase in Sec. III C 5. In Sec. III D 1 we demonstrate the absence of vector-chiral order in the two-component LL phases, and in Sec. III D 2 we show that one of them is a spin-nematic LL. In Sec. IV we discuss in detail the transition from the magnetized dimer phase to the magnetized Haldane phase, which we identify to be an Ising transition with central charge $c = 1 + 1/2 = 3/2$. This scenario is further corroborated by a field-theoretical treatment in the vicinity of the TB point discussed in Sec. V. We summarize our findings and conclude in Sec. VI. Finally, we provide in Appendixes A and B a more detailed discussion of the BA solutions of the model at the TB and the ULS point at finite magnetic fields, respectively.

II. OBSERVABLES AND CORRELATION FUNCTIONS

A. Magnetization

The properties of the model have been identified by calculating with DMRG a number of characteristic quantities. The first one is the magnetization defined by

$$M = \frac{1}{L}\sum_i \langle S_i^z \rangle, \tag{2}$$

which has been determined as a function of θ and applied magnetic field H [Fig. 1(a)].

B. Spin-correlation functions

The second source of information comes from the behavior of correlation functions characterizing magnetic, spin-nematic, and vector-chiral (quasi-)long-range order. We investigate possible algebraic decay of these correlation functions and compare the numerical values of the exponents with each other, the exponent with the smallest absolute value giving the dominant correlation function. This is of particular interest for the characterization of the gapless LL phases at finite field.

The first type of QLRO is identified by the correlation functions of the local spins,

$$C_S^{\text{long}}(i,j) = \langle S_i^z S_j^z \rangle - \langle S_i^z \rangle \langle S_j^z \rangle, \tag{3}$$

$$C_S^{\text{trans}}(i,j) = \langle S_i^- S_j^+ \rangle. \tag{4}$$

In one dimension, an algebraic decay of $C_S^{\text{long}}(i,j)$ indicates magnetic QLRO along the field, while a power-law behavior of $C_S^{\text{trans}}(i,j)$ can be interpreted as magnetic QLRO perpendicular to the field or as a quasicondensate of magnons.

C. Quadrupolar correlation functions

For systems with $S > 1/2$, however, QLRO can also be identified by considering the on-site spin-nematic correlation functions

$$C_Q(i,j) = \langle \vec{Q}_i \cdot \vec{Q}_j \rangle - \langle \vec{Q}_i \rangle \cdot \langle \vec{Q}_j \rangle, \tag{5}$$

where we have introduced the local quadrupolar order parameter

$$\vec{Q}_i = \begin{pmatrix} \frac{2}{\sqrt{3}}\left[\left(S_i^z\right)^2 - \frac{1}{4}\left(S_i^+ S_i^- + S_i^- S_i^+\right) \right] \\ \frac{1}{2}\left(S_i^+ S_i^z + S_i^z S_i^+ + S_i^- S_i^z + S_i^z S_i^-\right) \\ -\frac{i}{2}\left(S_i^+ S_i^z + S_i^z S_i^+ - S_i^- S_i^z - S_i^z S_i^-\right) \\ -\frac{i}{2}\left[\left(S_i^+\right)^2 - \left(S_i^-\right)^2 \right] \\ \frac{1}{2}\left[(S_i^+)^2 + (S_i^-)^2 \right] \end{pmatrix}. \tag{6}$$

Note that only the first entry of this vector conserves S^z_{total}, while the other ones change this quantum number by $\Delta S^z = 1$ or $\Delta S^z = 2$, respectively. This leads to three components of the correlation functions (5): the longitudinal component $C_{Q,0}$ considering the terms conserving S^z_{total}, the transverse component $C_{Q,1}$ considering the entries of Eq. (6) with $\Delta S^z = \pm 1$, and the pairing component $C_{Q,2}$ considering the entries with $\Delta S^z = \pm 2$. In particular, we compute

$$C_{Q,0}(i,j) = 2\big(\tfrac{1}{12}\big\langle \big[S_i^- S_i^+ + S_i^+ S_i^- - 4\left(S_i^z\right)^2\big] \times \big[S_j^- S_j^+ + S_j^+ S_j^- - 4\left(S_j^z\right)^2\big]\big\rangle - \langle Q_i^{(1)}\rangle\langle Q_j^{(1)}\rangle\big), \tag{7}$$

$$C_{Q,1}(i,j) = \tfrac{1}{2}\big\langle \left(S_i^+ S_i^z + S_i^z S_i^+\right)\left(S_j^z S_j^- + S_j^- S_j^z\right) + \text{H.c.}\big\rangle, \tag{8}$$

$$C_{Q,2}(i,j) = \tfrac{1}{2}\langle (S_i^+)^2 (S_j^-)^2 + \text{H.c.}\rangle. \tag{9}$$

At zero magnetic field, these three components are identical due to the SU(2) symmetry of the system. At finite field, however, the SU(2) symmetry is reduced to U(1) and the different components can show different behavior and characterize different types of QLRO. In addition, in the presence of a finite field, the operators entering C_S^{long} and $C_{Q,0}$ are allowed to mix by symmetry. These correlation functions are thus expected to decay with the same power law and to test for the same type of QLRO, namely magnetic QLRO along the field. Similarly, C_S^{trans} and $C_{Q,1}$ can mix and test for magnetic QLRO transverse to the field, or for magnon quasicondensation. However, the pairing component $C_{Q,2}$ has no magnetic partner and probes possible QLRO of nonmagnetic type. In the following we will refer to a phase at finite magnetizations in which this component decays algebraically and dominates as a quadrupolar or *spin-nematic Luttinger liquid*. In analogy to the interpretation of Eq. (4), QLRO in $C_{Q,2}$ can also be viewed as the quasicondensation of $S = 2$ bound pairs of magnons. If, in addition, the structure factor of this component of the quadrupolar correlation function is peaked at a wave vector $q = 0$, we call the phase a *ferroquadrupolar Luttinger liquid*, which we sketch in Fig. 2: on a single site, a finite expectation value $\langle \vec{Q}_i \rangle$ can be envisaged as fluctuations around an axis called *director*.[4] In a ferroquadrupolar phase, all directors align

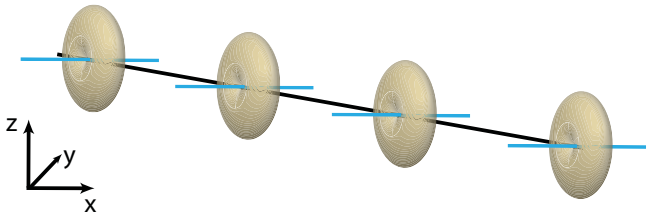

FIG. 2. (Color online) Sketch of a ferroquadrupolar ordered state in zero magnetic field. Note that the breaking of the spin-SU(2) symmetry can be described by a director located on each lattice site around which the spins fluctuate. The parallel alignement of these directors perpendicular to the z axis is representative for the ferroquadrupolar state.

parallel to each other. Note that the directors are perpendicular to the field. In previous work, ferroquadrupolar long-range order has been identified for the $S = 1$ bilinear-biquadratic Heisenberg model on the square[35] and triangular lattice[4] at zero magnetic field. In the one-dimensional (1D) case, at zero field spin-nematic phases have been identified numerically.[24,36] They are not of ferroquadrupolar type since the structure factor is peaked at some finite momentum. However, in Sec. III C 3 we demonstrate that such a phase is realized in one dimension in the BLBQ chain in a magnetic field. Note that beyond the quadrupolar order it is possible to realize multipolar (quasi-)long-range order in spin systems by considering bond products of spin operators as described in Refs. 37–40. However, in the following we will restrict ourselves to the investigation of possible quadrupolar order.

D. Vector-chiral correlation functions

In addition to possible QLRO associated to breaking the SU(2) or U(1) symmetry, true LRO can be obtained by breaking the parity of the system. This is tested by the first of the following two vector-chiral correlation functions:

$$\begin{aligned} C_\kappa^{\text{long}}(i,j) &= \langle \kappa_i^z \kappa_j^z \rangle, \\ C_\kappa^{\text{trans}}(i,j) &= \langle \kappa_i^x \kappa_j^x \rangle = \langle \kappa_i^y \kappa_j^y \rangle, \\ \text{where } \vec{\kappa}_j &= \mathbf{S}_j \times \mathbf{S}_{j+1}. \end{aligned} \tag{10}$$

Such vector-chiral order has been, e.g., identified using the DMRG in frustrated $S = 1/2$ and $S = 1$ Heisenberg chains.[40,41] In this paper, we consider a proposal of Kolezhuk and Vekua[34] in which a vector-chiral phase at finite magnetizations for positive values of θ has been suggested. We address this issue by directly computing the correlation functions (10).

E. Correlation exponents

Whenever one of the above correlation functions decays as a power law at long distance, the decay will be described by a positive exponent η according to

$$C(i,j) \propto |i-j|^{-\eta}. \tag{11}$$

The exponents will be distinguished by the same indices and superscripts as the corresponding correlation functions: η_S^{long}, η_S^{trans}, $\eta_{Q,0}$, $\eta_{Q,1}$, $\eta_{Q,2}$. If several Fourier components of the

correlation functions decay algebraically, the exponents will be distinguished by an additional index.

As pointed out above, in a magnetic field some spin and quadrupolar correlation functions are coupled, so that $\eta_S^{\text{long}} = \eta_{Q,0}$ and $\eta_S^{\text{trans}} = \eta_{Q,1}$. So we end up with three *a priori* independent exponents: η_S^{long}, η_S^{trans}, and $\eta_{Q,2}$.

F. Central charge

The analysis of the phase diagram is complemented by computing the central charge c. For systems amenable to a description by conformal field theory this quantity characterizes the phase and the universality class of phase transitions.[42] Using the DMRG, it can be obtained easily by computing the von Neumann entanglement entropy of blocks of consecutive sites,

$$S_\ell = -\text{Tr}\varrho_\ell \ln \varrho_\ell, \tag{12}$$

where ϱ_ℓ is the reduced density matrix of a subsystem of size ℓ. In order to circumvent the oscillations that appear in the case of open boundary conditions (see Refs. 36 and 43 for the behavior at the TB and at the ULS points at zero field), we obtain c from systems with periodic boundary conditions (PBCs), for which Calabrese and Cardy[44] have derived the general expression

$$S_\ell = \frac{c}{3}\ln\left[\frac{L}{\pi}\sin\left(\frac{\pi\ell}{L}\right)\right] + g_{\text{PBC}}. \tag{13}$$

The numerical value of c is then obtained by computing S_ℓ for finite systems and fitting Eq. (13) to the results.

III. PHASE DIAGRAM OF THE BLBQ CHAIN AT FINITE MAGNETIC FIELDS

In this section, we map out the phase diagram by successively looking at the magnetization, the central charge, and the correlation functions.

A. Magnetization

The magnetization is depicted in Fig. 1(a). Three separate regions of magnetization can be identified. Starting from the dimerized phase, the magnetization of the finite systems grows regularly in steps of $\Delta M = 2/L$, similar to the behavior in certain polarized $S = 1/2$ magnetic systems.[37–40,45–47] This is rather natural. Indeed, in this parameter range (large negative biquadratic interactions), the system dimerizes to form singlet pairs, and the quintuplet crosses the triplet when the bilinear interaction vanishes. In this region, the first excitation of a pair of spins to cross the singlet upon applying a magnetic field is a quintuplet with $S^z = 2$, leading to the step size of $2/L$. In contrast to this, in an intermediate region around the Heisenberg point $\theta = 0$ the magnetization grows in steps of $\Delta M = 1/L$. In the region $-\pi/4 \leqslant \theta \lesssim -\pi/10$ the results for finite systems indicate a line of transitions at which the magnetization steps change from $\Delta M = 2/L$ to $\Delta M = 1/L$ upon increasing θ and keeping $H = \text{const}$, or upon increasing H at constant θ, indicating the presence of a phase transition. This phase transition will be discussed in detail in Sec. IV. By further increasing θ, we identify a kink anomaly developing at $\theta \gtrsim \pi/9$ and persisting up to $\theta = \pi/2$. Its position on the magnetization curve grows quickly up to the ULS point and then seems to saturate at $M \approx 0.6$, in agreement with previous findings concentrating on the Haldane phase (Refs. 29 and 30) and the vicinity of the ULS point (Refs. 28 and 31).

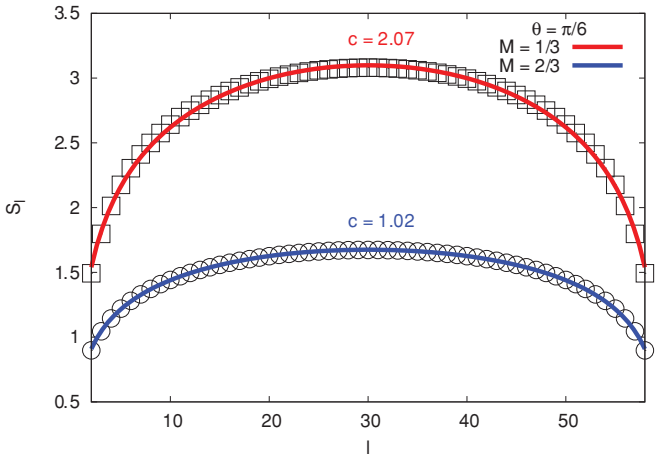

FIG. 3. (Color online) Block entropy for a system with $L = 60$ lattice sites and PBC at $\theta = \pi/6$ below the kink transition ($M = 1/3$, □) and above ($M = 2/3$, ◯). The solid lines indicate the fit with Eq. (13); the labels denote the central charge obtained by this fit.

B. Central charge

The central charge has been calculated throughout the phase diagram. It is equal to 2 below the kink, and equal to 1 everywhere else (except along the transition line where the magnetization steps change from $\Delta M = 2/L$ to $\Delta M = 1/L$, where it is equal to 3/2; see below). Typical results are plotted in Fig. 3.

When the central charge is equal to 1, the system is a single component Luttinger liquid, and all correlation exponents are controlled by a single parameter, leading to specific relationships between the exponents of algebraic correlations. When the central charge is equal to 2, the system is a two-component Luttinger liquid, and the exponents of the algebraic correlations can be obtained from the dressed charge matrix (see Appendix B).

So magnetization and central charge reveal the presence of three main phases: two single-component Luttinger liquid phases with magnetization steps $\Delta M = 2/L$ and $\Delta M = 1/L$, respectively, and a two-component Luttinger liquid phase. We now turn to a careful investigation of correlations inside these phases to identify the nature of the dominant correlations.

C. Correlation functions in the single-component Luttinger liquid phases

In this and the following section we base the characterization of the phases on the values of the exponents of $C_{Q,2}$, C_S^{trans}, and C_S^{long}. It is sufficient to consider only these correlation functions since, as expected due to the mixing at finite field, we find that transverse or longitudinal correlation functions decay with the same exponent, respectively. An exception to this is the longitudinal component of the vector-chiral

correlation function, which we find to decay with an exponent of approximately 2 for all values of M and θ.

The behavior of the exponents reveals important aspects of the phase diagram: As seen in Figs. 4(b) and 4(c), the transverse correlation functions decay algebraically with an exponent whose absolute value is much smaller than $\eta_{Q,2}$, as soon as the size of the magnetization steps changes to $\Delta M = 1/L$, revealing a fundamental change in the physics despite the fact that the central charge on both sides of the transition is $c = 1$. The critical value of θ at which this transition takes place depends on the magnetization. This scenario is reminiscent of the paired superfluid phase and pair-unbinding transition to a superfluid of single bosons identified in Ref. 48 for systems of hard-core bosons with correlated hopping on the square lattice. At the present, it is unclear if in this system the transition is of first or second order. In the case of the BLBQ chain, however, we identify the transition to be a continuous one as we discuss in detail in Sec. IV. In the following, we address the various aspects concerning the correlation functions and the physics they reveal in more detail.

1. *Exponent of the transverse correlation functions*

In the discussion of the phase diagram, we mainly consider the exponents η_S^{trans} and $\eta_{Q,2}$. This is possible since we identify both, from the numerical data as well as from a field-theory and Bethe ansatz approach (see Sec. V and Appendix A), that the exponent η_S^{long} in the single-channel LL phases is the inverse of the one of the corresponding transverse correlation function, i.e., $\eta_S^{\text{long}} = 1/\eta_{Q,2}$ in the magnetized dimer phase and $\eta_S^{\text{long}} = 1/\eta_S^{\text{trans}}$ in the magnetized Haldane phase. Note, however, that the longitudinal correlation functions possess an additional oscillating component, which makes it more difficult to obtain the numerical value of the exponent with a high precision. In order to obtain accurate results, we fit the exponent η_S^{long} to the Friedel oscillations in the local spin density $\langle S_i^z \rangle$ using expressions obtained by bosonization, as discussed in Sec. V below. We apply Eq. (35) in the magnetized Haldane phase and Eq. (41) in the magnetized dimer phase by performing the fit only in the bulk region around the center of the system. We find that in the magnetized Haldane phase close to the transition to the ferroquadrupolar LL, finite-size effects become predominant due to the vicinity of the critical point. However, in contrast to the approach used in Ref. 49, using these expressions it is possible to obtain accurate results without introducing additional phenomenological fitting parameters. Note that in the region where $c = 2$, there is no simple relation between the exponents of the various correlation functions, as discussed in more detail in Appendix B. However, we find this exponent to be larger than η_S^{trans} and $\eta_{Q,2}$, so we conclude that the longitudinal correlations do not become dominant in the two-channel LL region.

2. *Oscillatory component of the longitudinal correlation functions*

We find that in the magnetized Haldane phase the oscillatory component of the longitudinal correlations decays faster at larger magnetizations, and substantially faster than in the ferroquadrupolar LL phase. The frequency of this oscillation

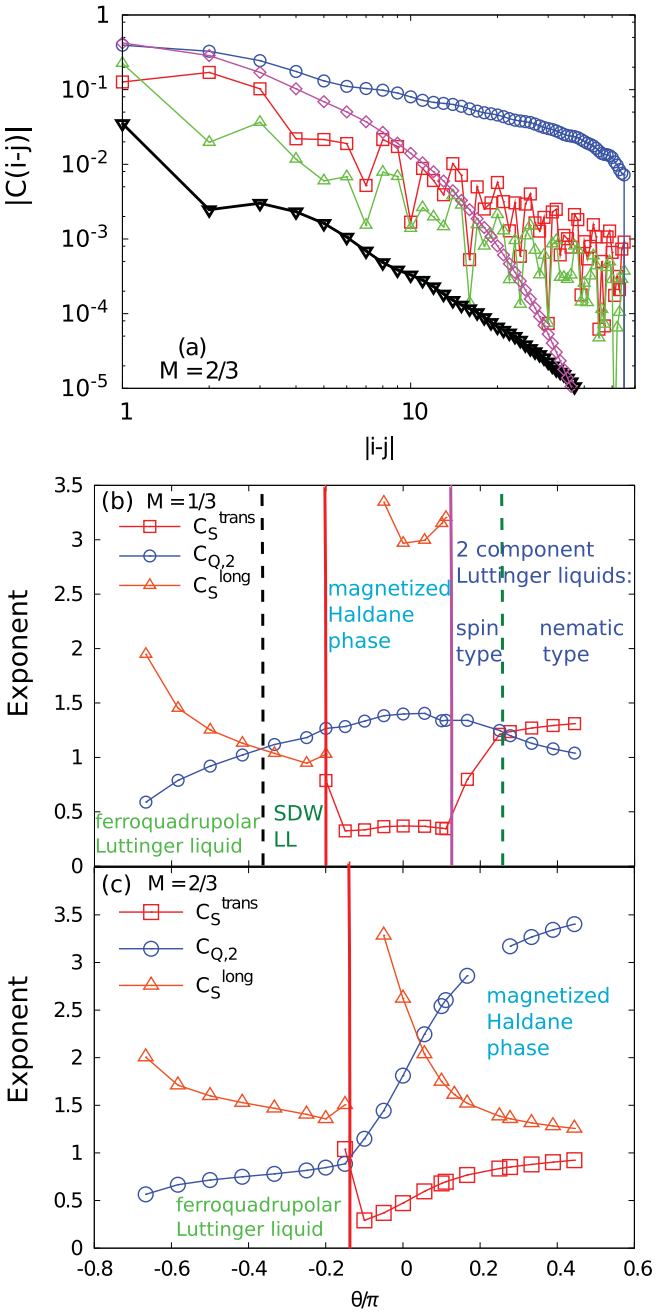

FIG. 4. (Color online) (a) Absolute value of the algebraically decaying correlation functions in the ferroquadrupolar LL phase at $M = 2/3, \theta = -0.2\pi$. The symbols and colors indicate C_S^{long} [Eq. (3), red line, □], $C_{Q,0}$ [Eq. (7), green line, △] and $C_{Q,2}$ [Eq. (9), blue line, ◯], and C_κ^{long} [Eq. (10), black line, ▽]. In addition, C_S^{trans} [Eq. (4), magenta line, ◇] - expected to decay exponentially - is shown. (b) Value of the exponents of C_S^{trans} [Eq. (4)], of $C_{Q,2}$ [Eq. (9)], and of C_S^{long} [Eq. (3)] as a function of θ at $M = 1/3$. (c) The same as in (b) but at $M = 2/3$. The vertical lines in (b) and (c) indicate the position of the phase transitions and crossovers as depicted in Fig. 1. Note that in the high field phase at $\theta = \pi/4$ the number of down spins is zero, leading to a vanishing $C_{Q,2}$. In (b) and (c) the value of η_S^{long} close to the phase transition at $\theta \approx -0.2\pi$ is not shown since it is strongly affected by finite size effects.

depends on the value of the magnetization, and changes upon crossing the phase transition. It is remarkable that the wave vector of these oscillations in the ferroquadrupolar LL phase is $\pi(1-M)$, while at the Heisenberg point it is $2\pi M$.[50,51] This can be understood in terms of the bound pairs of magnons populating the lattice, leading to an effective filling, which is only half the value of the magnetization. This aspect will be discussed in more detail in Sec. V in the context of a field-theoretical treatment.

3. Ferroquadrupolar Luttinger liquid phase

We now focus on the region of the phase diagram in which the magnetization steps are of size $\Delta M = 2/L$ at high magnetizations (the light green region in Fig. 1). In Fig. 4(a) we present our DMRG results for the various correlation functions as obtained for systems with $L = 60$ lattice sites with open boundary conditions at $M = 2/3$ and $\theta = -0.2\pi$, a case that is representative for this phase. The plot shows that the pairing component of C_Q decays slowest, consistent with a spin-nematic phase. Since the structure factor associated to this correlation function is peaked at a wave vector $q = 0$, and the central charge is found to be $c = 1$, we conclude that the system realizes a single-channel ferroquadrupolar LL phase. At the same time, the transverse spin-correlation function decays exponentially, showing that the single-spin excitation spectrum possesses a finite gap and that there is no quasicondensation of magnons. This interpretation is further confirmed by the analysis of the one-magnon and two-magnon spin gap, which is presented in more detail in Sec. IV below. In addition, a Bethe ansatz analysis at the integrable TB point confirms the numerical finding of a power-law decay in $C_{Q,2}$ at finite field, while the one-magnon sector acquires a gap (see Appendix A).

4. Crossover from a ferroquadrupolar Luttinger liquid to a spin-density-wave Luttinger liquid

In Fig. 5 we show the exponents of the correlation functions C_S^{long} and $C_{Q,2}$ as a function of the magnetization as obtained by Bethe ansatz at the TB point $\theta_{\text{TB}} = -\pi/4$. We observe that for magnetizations $M \lesssim 0.4$ the exponent of C_S^{long} is smaller than 1, while for larger magnetizations $C_{Q,2}$ becomes dominant. This is in agreement with numerical results for these exponents. Furthermore, we identify numerically for values of θ away from the integrable TB point the existence of a crossover line in the low-field region, which we show in Figs. 1(b) and 1(c). At this crossover, the dominant correlations change from spin-nematic ones at large magnetizations to spin-density-wave (SDW) correlations. This is similar to a scenario realized by a frustrated ferromagnetic $S = 1/2$ Heisenberg chain in a magnetic field, in which a crossover line divides spin-multipolar LL phases into a nematic and a SDW type of LL, as discussed in Refs. 37,39 and 40.

5. Magnetized Haldane phase

We find that the magnetized Haldane phase extends all over the region depicted in light blue in Fig. 1, i.e., up to values of $\theta = \pi/2$ in the high-field region above the kink transition. For the transverse spin correlations, the exponent can be obtained

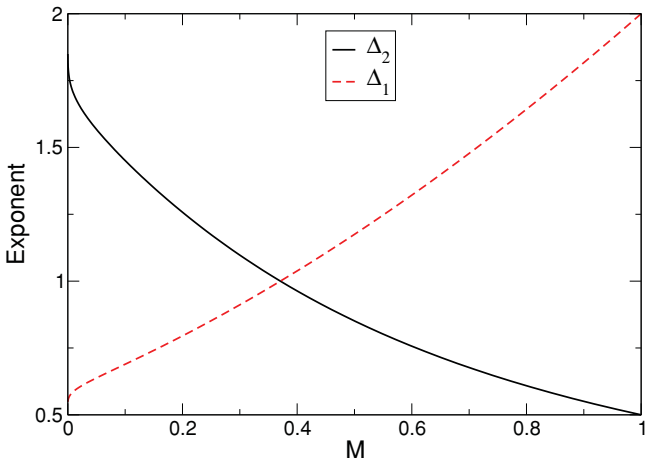

FIG. 5. (Color online) Exponents $\Delta_{1,2}$ of the power law decay of C_S^{long} and of $C_{Q,2}$, respectively, at the TB point ($\theta = -\pi/4$) as functions of the magnetization per site as obtained by Bethe ansatz (see Appendix A). For small magnetizations C_S^{long} characterized by the exponent Δ_1 dominates, while for large magnetization $C_{Q,2}$ characterized by the exponent Δ_2 becomes dominant.

with reliable accuracy and at the Heisenberg point the obtained numerical value compares well with previously published results.[49,50,52,53] In the whole phase, the numerical data indicate that $\eta_S^{\text{long}} = 1/\eta_S^{\text{trans}}$. Interestingly, $\eta_{Q,2} \approx 4\eta_S^{\text{trans}}$, as can be seen in Figs. 4(b) and 4(c). Both findings are in agreement with predictions from field theory presented in Sec. V. The exponent of C_Q at low magnetizations behaves rather smoothly at the transition. However, at larger magnetizations its magnitude increases quickly when crossing the phase transition, leading $C_{Q,2}$ to decay very fast in the high-field region of the magnetized Haldane phase. This can be related to the small number of down spins in that region. The same effect is responsible for the complete suppression of these correlations at the ULS point due to the absence of down spins at this point, which is discussed in Ref. 31 and in Appendix A.

Note that η_S^{trans} jumps at the transition from the magnetized Haldane phase to the ferroquadrupolar LL phase. This is due to the nature of the phase transition and can be explained in terms of a field-theory treatment of the transition, presented in Sec. V B 3.

With this we conclude the discussion of the single-component LL phases and turn now to the behavior of the correlation functions below the kink transition.

D. Correlation functions in the two-component Luttinger liquid phases

In this section, we turn to the phases realized below the kink transition and characterize them by identifying the dominant correlation functions.

1. Absence of vector-chiral order

The search for a parity broken phase is motivated by findings for frustrated $S = 1/2$ chains, in which a kink transition separates two single-channel LLs, one of them exhibiting vector-chiral order.[41] By analogy, it has been suggested that the

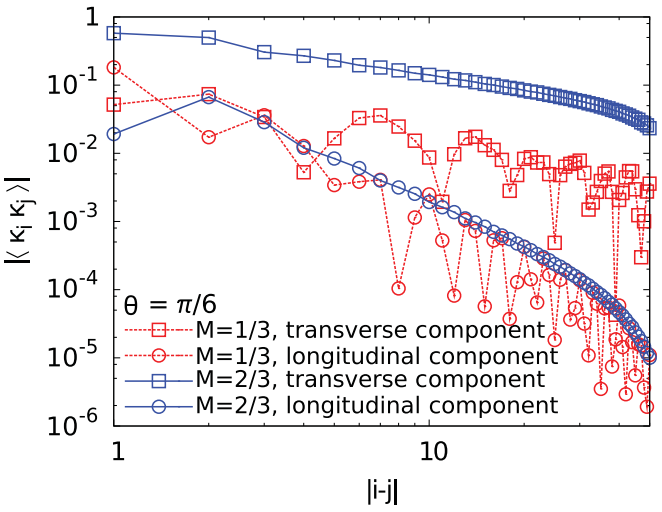

FIG. 6. (Color online) Vector-chiral correlation functions below ($M = 1/3$, dashed lines) and above ($M = 2/3$, solid lines) the kink transition at $\theta = \pi/6$.

same scenario might occur in the present bilinear-biquadratic $S = 1$ chain.[34] However, as discussed in Sec. III B, in the whole region below the kink the central charge is $c = 2$, supporting a scenario in which two-component LL physics without vector-chiral order is realized. This is confirmed by our results for the vector-chiral correlation functions shown in Fig. 6, which do not indicate the presence of parity breaking. We therefore conclude that vector-chiral order is not realized and that below the kink transition in the whole region two-channel LLs are realized, which we will further characterize in the next section.

2. *Crossover from a SDW to a spin-nematic two-channel Luttinger liquid*

As shown in Fig. 4(b), in the region $\pi/9 \lesssim \theta \lesssim \pi/4$ the transverse spin correlations are more dominant than the quadrupolar ones, while in the region $\pi/4 < \theta < \pi/2$ the quadrupolar correlations tend to be dominant. The presence of such a crossover line is confirmed by a Bethe ansatz analysis at the ULS point $\theta_{\rm ULS} = \pi/4$ presented in more detail in Appendix B. Note that the presence of the two massless modes leads to oscillating components at various momenta, which makes it difficult to obtain the numerical values of the exponents of the correlation functions. However, at the ULS point we can compare to the Bethe ansatz results; see Table I. The numerical values are obtained for $M = 1/3$, and a good agreement between the DMRG and the Bethe ansatz results is obtained.

As shown in Fig. 7, the Bethe ansatz results demonstrate that for $M \lesssim 0.258$ the spin-nematic correlations are dominant, while at larger fields the transverse spin correlations are dominant. A further numerical analysis of the exponents around $\theta = \pi/4$ indicates that the crossover line is, indeed, bent. It seems to exist at values $\theta < \pi/4$ for $M < 0.25$, while for $M > 0.25$ it seems to exist at $\theta > \pi/4$, but bending back toward $\pi/4$ upon further increasing M. However, since the values of the exponents are so close, it is very difficult to identify the exact position of this crossover line numerically and therefore we leave this aspect for future investigations.

TABLE I. Comparison of the values for the exponents of the various correlation functions at the ULS point $\theta_{\rm ULS} = \pi/4$ at $M = 1/3$ as obtained by DMRG and Bethe ansatz. We display the exponents of the nonoscillatory part, $k = 0$, and the two smallest values at finite wave vectors k_1 and k_2.

	$k = 0$	k_1	k_2
Longitudinal correlations:			
$C^S_{\rm long}$	1.91	1.75	1.77
$C_{Q,0}$	1.75	1.58	1.71
Bethe ansatz	2	1.60	1.63
Transverse correlations:			
$C^S_{\rm trans}$		1.37	1.51
$C_{Q,1}$		1.38	1.51
Bethe ansatz		1.18	1.28
Spin-nematic correlations:			
$C_{Q,2}$	1.61	1.38	
Bethe ansatz	1.68	1.20	

Due to this crossover line, the system seems to reflect to some extent the behavior at zero field, where the system is in the gapped Haldane phase for $\theta < \pi/4$, but realizes an antiferroquadrupolar $c = 2$ critical state for $\theta > \pi/4$.[24] Note that this spin-nematic LL is not a ferroquadrupolar LL since the structure factor of the quadrupolar correlations is not peaked at a wave vector $q = 0$, but at wave vectors that depend both on the value of θ and on the strength of the magnetic field H, as discussed in Ref. 31 and in Appendix B.

Summarizing all these findings, we obtain the magnetic-phase diagram of the BLBQ $S = 1$ Heisenberg chain presented in Figs. 1(b) and 1(c). In the next section, we will discuss in

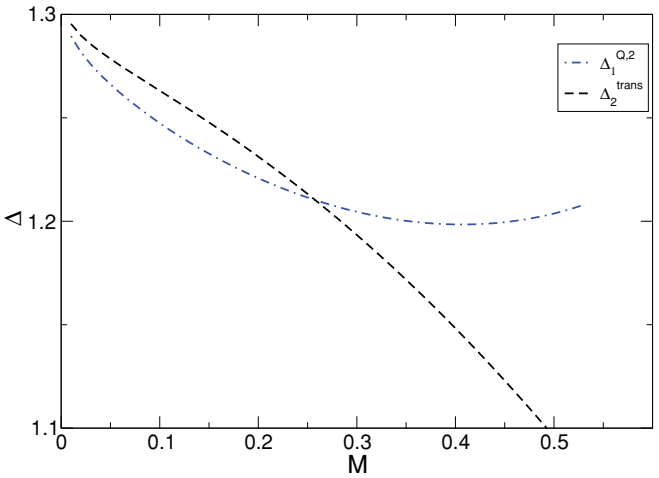

FIG. 7. (Color online) Bethe ansatz results for the exponents of the dominant component of the correlations at the ULS point $\theta_{\rm ULS} = \pi/4$ in the 2 LL region below the kink. The results shown are obtained by the Bethe ansatz calculation presented in Appendix B and show the smallest values of the exponents of $C^{\rm trans}_S$ and $C_{Q,2}$ as a function of the magnetization per site. We observe a crossover between a regime where transverse spin correlations and quadrupolar correlations are dominant at $M \approx 0.258$. Note that the exponents of the other components of the correlations are larger and are discussed in more detail in Appendix B.

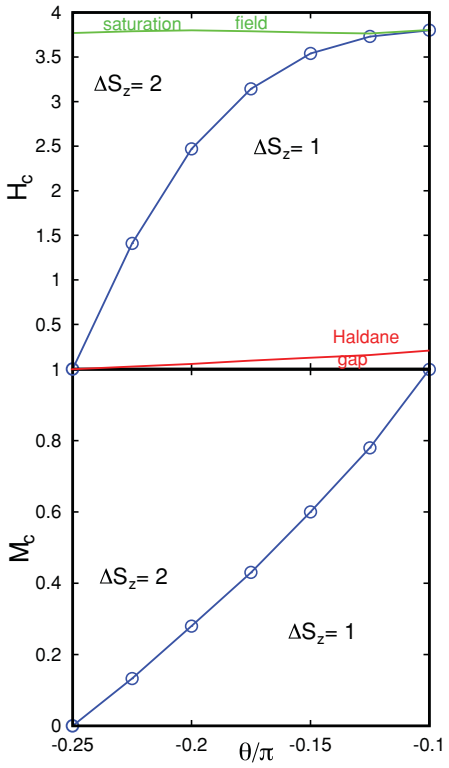

FIG. 8. (Color online) Line of phase transitions between the ferroquadrupolar LL and the magnetized Haldane phase (a) as a function of (H,θ) and (b) as a function of (M,θ). The data points indicate the position at which the step size of the magnetization changes from $\Delta M = 2/L$ to $\Delta M = 1/L$ for systems with $L = 120$ lattice sites.

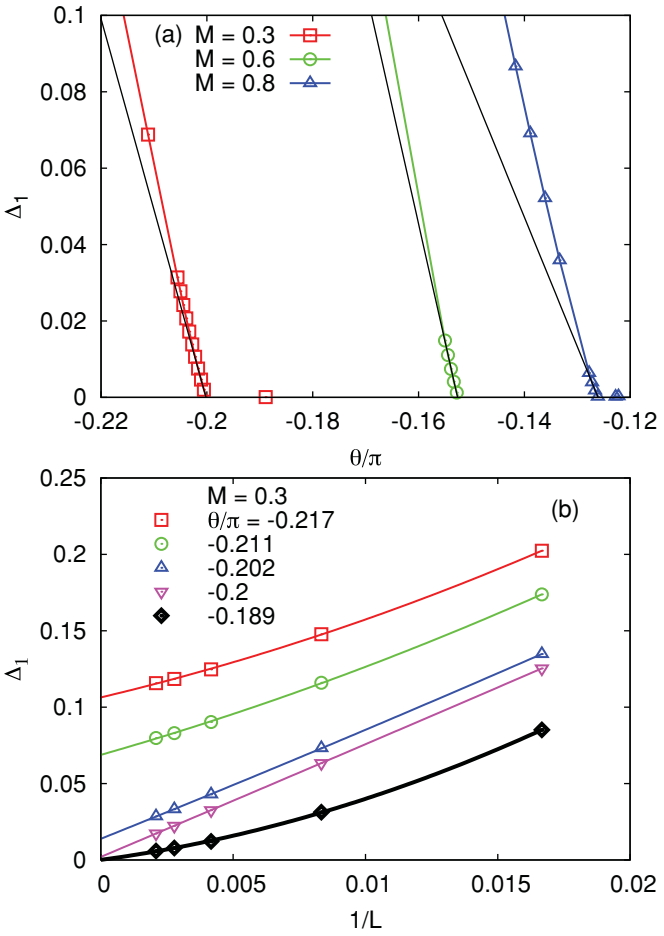

FIG. 9. (Color online) (a) $\Delta_1(\theta)$ at $M = 0.3$, $M = 0.6$, and $M = 0.8$ after extrapolation to the thermodynamic limit. The black lines are linear fits in the vicinity of the critical points. (b) Example of the finite-size scaling of the gap as a function of $1/L$ at $M = 0.3$. The solid lines are fits with second-order polynomials and are shown as a guide to the eye.

detail the nature of the transition from the ferroquadrupolar LL to the magnetized Haldane phase at finite magnetizations.

IV. PAIR-UNBINDING TRANSITION

In this section, we focus on the nature of the phase transition between the ferroquadrupolar LL and the magnetized Haldane phase. By considering systems with up to $L = 480$ lattice sites, we do not find any indication for the formation of a jump in the magnetization curve, showing that a continuous rather than a first-order transition (metamagnetic transition) is taking place. Our findings for the magnetization curves indicate that an infinitesimal magnetic field at the TB point leads immediately to the binding of two magnons, while for $\theta > \theta_{\mathrm{TB}}$ closing of the Haldane gap leads to the condensation of single magnons. On the other hand, for the fully polarized state, decreasing the field will lead to such bound states in the region $\theta \leqslant \arctan(-1/3)$,[54] while for larger values of θ the excitations of the fully polarized state are described by single magnons. We therefore conclude that the line of transitions is located between the TB point at zero field and $-\theta_{\mathrm{AKLT}}$ at the saturation field, as shown in more detail in Fig. 8. In the following we provide further support that this transition is a continuous one. We consider the gaps

$$\Delta_1 = \tfrac{1}{2}[E_0(S_z+1) + E_0(S_z-1) - 2E_0(S_z)], \quad (14)$$

$$\Delta_2 = \tfrac{1}{2}[E_0(S_z+2) + E_0(S_z-2) - 2E_0(S_z)], \quad (15)$$

which have been applied in Ref. 37 for characterizing frustrated ferromagnetic $S = 1/2$ chains at finite magnetizations. Δ_1 is a measure for the energy of single-spin excitations, while Δ_2 correspondingly characterizes two-spin excitations. If $\Delta_2 < \Delta_1$, then the lowest-lying excitations are characterized as pairs of spins. We find that, after extrapolating to the thermodynamic limit, Δ_2 is always zero for all values of the magnetization in this parameter region. This is confirmed by the observed algebraic decay of the quadrupolar correlation functions all over the parameter range. However, Δ_1 is finite in the upper part of the magnetization curves, but becomes zero at the point where the step size of the magnetization curves changes, and remains zero in the magnetized Haldane phase. In Fig. 9 we show results for $\Delta_1(\theta)$ after extrapolating to the thermodynamic limit at three different values of the magnetization $M = 0.3$, $M = 0.6$ and $M = 0.8$. In all three cases, to a good approximation the gap in the vicinity of the transition point closes linearly and remains zero after the transition. This supports the scenario of a line of continuous phase transitions.

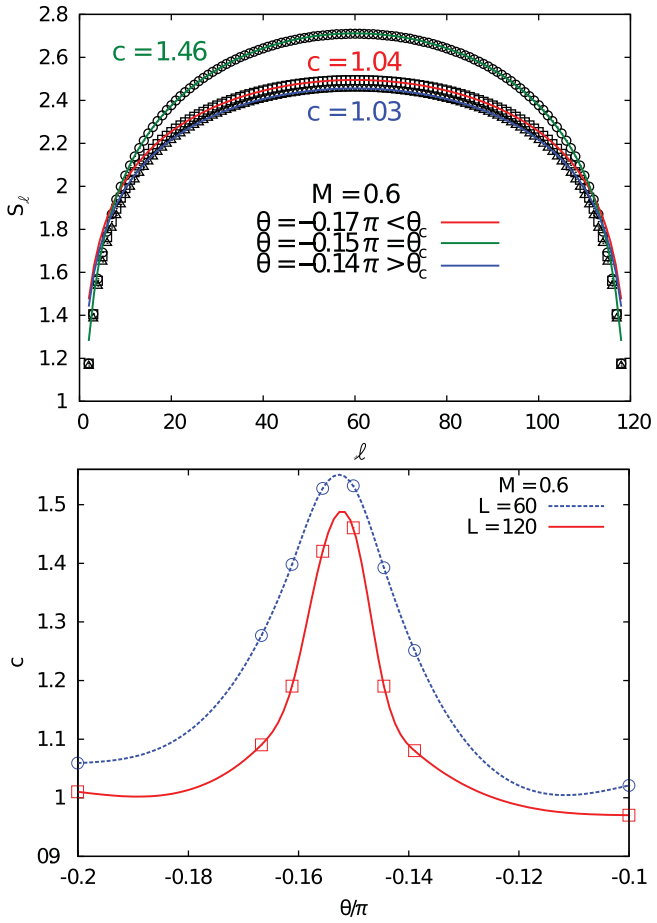

FIG. 10. (Color online) (a) Block entropy as obtained for systems with $L = 120$ lattice sites with PBC at $\theta \approx -0.17\pi < \theta_c$ (□), $\theta \approx -0.15\pi \approx \theta_c$ (○) and $\theta \approx -0.14\pi > \theta_c$ (△) at $M = 0.6$. The value of the central charge as obtained by fitting with Eq. (13) is shown. (b) Central charge as a function of θ for systems with $L = 60$ and $L = 120$ sites with PBC. The data points are connected by a spline interpolation as a guide to the eye. In the thermodynamic limit the maximum will be a sharp peak located at the critical point.

Next we address the universality class of the transition by computing the central charge c on the line of phase transitions and in the adjacent phases. In Fig. 10 we show our results for the block entropy for systems with PBC and $L = 60$ or $L = 120$ lattice sites keeping up to $m = 2000$ density matrix eigenstates. The value of the central charge is obtained by applying Eq. (13) for different values of θ at fixed magnetization $M = 0.6$. At the critical point, we obtain a value close to $c = 3/2$, which is reproduced everywhere on the critical line, while we find the expected $c = 1$ in both the ferroquadrupolar LL phase and the magnetized Haldane phase.

It is remarkable that the measured effective central charge at the transition in finite field is the same as the one at zero field at the TB point. In this case the transition belongs to the $SU(2)_{k=2}$ Wess-Zumino-Witten-Novikov (WZWN) class,[55] with a unique set of scaling dimensions (and therefore exponents of the correlation functions).

The nature of the transition in a finite field is discussed in some detail using field-theory methods in Sec. V. In particular it is shown there that the value $c = 3/2$ for the central charge arises from an Ising degree of freedom that becomes critical on top of an already present critical Luttinger liquid, i.e., $3/2 = 1 + 1/2$. This is analogous to what has been found in Ref. 56 for a transition between two superfluids in a two-component bosonic Feshbach problem, and in Refs. 57–61 for the case of a fermionic $S = 3/2$ Hubbard model. In the attractive $S = 3/2$ Hubbard model the Ising transition separates a quasicondensate of pairs and a quasicondensate of quartets of fermions. This is reminiscent of our findings for the BLBQ chain in which the phase transition is connecting a quasicondensate of magnons in the magnetized Haldane phase with the quasicondensate of pairs of magnons in the ferroquadrupolar LL phase, relating a single magnon in the BLBQ chain to pairs of fermions in the $S = 3/2$ Hubbard model.

It would be interesting to identify the Z_2 symmetry of the Hamiltonian which gets broken at such pair-unbinding transitions. In higher dimensions, the U(1) symmetry of the system can be broken down partially to Z_2, and this remaining discrete symmetry can further spontaneously break at the phase transition (see, e.g., Ref. 62). However, in one dimension, the continuous U(1) symmetry cannot be broken, and identifying the Z_2 symmetry is a more difficult task. This goes beyond the scope of the present paper in which we focus on presenting evidence in favor of such a scenario in the BLBQ chain at finite fields, and we leave a further characterization of this aspect open for future research.

The Ising transition encountered in the models mentioned above can be characterized by considering particular *ratios* of correlation functions.[57] It is shown in Sec. V that

$$R(|i-j|) = \frac{\langle S_i^- S_j^+ \rangle^4}{C_{Q,2}(i,j)} \tag{16}$$

can be used as a diagnostic of the Ising transition. More precisely, the ratio $R(|i-j|)$ is related to a two-point function of an Ising disorder field $\mu(x)$ by

$$R(|i-j|) \propto= \langle \mu(x)\mu(0)\rangle^4. \tag{17}$$

The magnetized Haldane phase corresponds to the disordered phase of the Ising model, so that $\langle \mu(x)\rangle \neq 0$ and hence R is expected to tend to a finite value. On the other hand, the ferroquadrupolar LL phase corresponds to the ordered Ising phase and hence R will decay exponentially. At the transition itself the field theory predicts $R(|i-j|) \sim 1/|i-j|$.

In Fig. 11(a), we show our results for R at fixed value of the magnetization when changing θ. In the ferroquadrupolar LL phase, this quantity decays exponentially, while in the magnetized Haldane phase it indeed tends to a finite value. At criticality, it decays $\sim 1/|i-j|$. Note that in this case the value of one or both exponents of the correlation functions needs to jump at the transition. As we will see in Sec. V, it is the exponent of C_S^{trans} which behaves discontinuously, in agreement with the results shown in Figs. 4(b) and 4(c). In Fig. 11(b), we show the value of $R(|i-j| = 30)$ and $R(|i-j| = 50)$ as a function of θ at various values of the magnetization. Even though we are not considering the limit of infinite separation between i and j, the behavior at the critical point is linear to a good approximation.

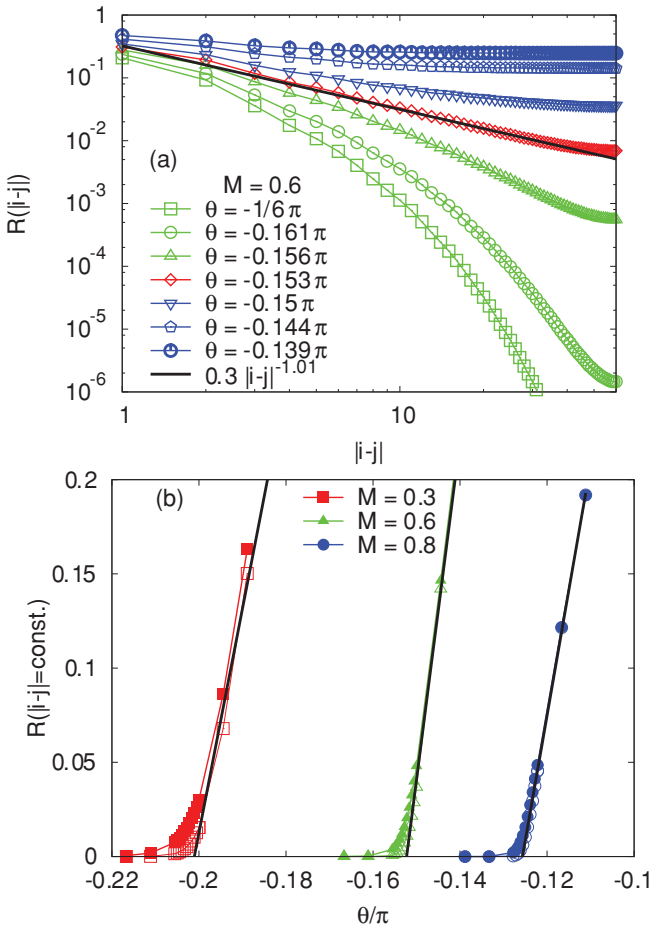

FIG. 11. (Color online) (a) Ratio $R(|i-j|)$ [Eq. (16)] as a function of θ at $M = 0.6$. (b) Value of $R(30)$ (thick lines, filled symbols) and $R(50)$ (thin lines, empty symbols) as a function of θ at $M = 0.3$, $M = 0.6$, and $M = 0.8$ obtained for systems with $L = 120$ lattice sites and PBC. The black lines are linear fits in the vicinity of the critical points.

Finally, we may consider the scaling of the Ising order parameter $\langle\mu(0)\rangle$ as a function of the deviation $\theta - \theta_c$ from the critical point. As is shown in the next section, this is related to R by

$$\lim_{|i-j|\to\infty} R(|i-j|,\theta) \propto \langle\mu(0)\rangle^8 \propto |\theta - \theta_c|. \tag{18}$$

Hence the linear behavior shown in Fig. 11(b) is also in agreement with an Ising transition. Additional support for this scenario is given by comparing the values of the critical points obtained by a linear extrapolation of $R(30)$ and by a linear fit to $\Delta_1(\theta)$. From both sets of data, at $M = 0.3$ we obtain $\theta_c \approx -0.2$, at $M = 0.6$ we obtain $\theta_c \approx -0.15$, and at $M = 0.8$ we find $\theta_c \approx -0.125$. Hence we conclude that starting from the TB point at zero field, on the emerging line of phase transitions the value of $c = 3/2$ is kept, but the universality class changes from $SU(2)_{k=2}$ WZWN to Luttinger liquid plus Ising. This agrees with the picture emerging from the field-theoretical treatment of this transition, which we present in the next section.

V. FIELD THEORY IN THE VICINITY OF THE ISING TRANSITION

Following Tsvelik[63] we can construct a field-theory description of the model in the vicinity of the Takhtajan-Babujian point $\theta_{TB} = -\frac{\pi}{4}$, $H = 0$. This results in a Hamiltonian of the form

$$\mathcal{H} = \frac{iv}{2}\sum_{a=1}^{3} L_a\partial_x L_a - R_a\partial_x R_a - im\sum_{a=1}^{3} R_a L_a + iH[L_1L_2 + R_1R_2] + g\sum_{a=1}^{3} J^a J^a, \tag{19}$$

where L_a and R_a are left- and right-moving Majorana fermions and

$$J^a = -\frac{i}{2}\epsilon^{abc}[L_bL_c + R_bR_c]. \tag{20}$$

The mass m in Eq. (19) is proportional to the deviation $\theta - \theta_{TB}$ from the Takhtajan-Babujian point. The lattice spin operators are expressed in terms of continuum fields as

$$S_j^a \sim M^a(x) + (-1)^j n^a(x), \tag{21}$$

where $x = ja_0$ (a_0 is the lattice spacing). Here M^a are related to the currents $M^a(x) \propto J^a(x)$, while $n^a(x)$ are expressed in terms of the Ising order and disorder operators as

$$\begin{aligned} n^x(x) &\propto \sigma^1(x)\mu^2(x)\mu^3(x),\\ n^y(x) &\propto \mu^1(x)\sigma^2(x)\mu^3(x),\\ n^z(x) &\propto \mu^1(x)\mu^2(x)\sigma^3(x). \end{aligned} \tag{22}$$

We may bosonize the Majoranas 1 and 2 using

$$\begin{aligned} i[R_1L_1 + R_2L_2] &\sim \frac{1}{\pi\alpha}\cos\sqrt{4\pi}(\varphi_R + \varphi_L),\\ i[L_1L_2 + R_1R_2] &\sim \frac{1}{\sqrt{\pi}}\partial_x(\varphi_R + \varphi_L),\\ L_1 + iL_2 &\sim \frac{1}{\sqrt{\pi\alpha}}e^{-i\sqrt{4\pi}\varphi_L},\\ R_1 + iR_2 &\sim \frac{1}{\sqrt{\pi\alpha}}e^{i\sqrt{4\pi}\varphi_R}. \end{aligned} \tag{23}$$

Here α is a short-distance cutoff. Rewriting the Hamiltonian (19) in terms of the canonical Bose field $\Phi = \varphi_L + \varphi_R$ and the dual field $\Theta = \varphi_L - \varphi_R$ results in

$$\begin{aligned} \mathcal{H} &= \mathcal{H}_3 + \mathcal{H}_B + \mathcal{H}_{\rm int},\\ \mathcal{H}_3 &= \frac{iv}{2}[L_3\partial_x L_3 - R_3\partial_x R_3] - im\, R_3L_3,\\ \mathcal{H}_B &= \frac{v'}{2}\left[\frac{1}{K}(\partial_x\Phi)^2 + K(\partial_x\Theta)^2\right] - \frac{m}{\pi\alpha}\cos\sqrt{4\pi}\Phi + \frac{H}{\sqrt{\pi}}\partial_x\Phi,\\ \mathcal{H}_{\rm int} &= \frac{2ig}{\pi\alpha}\cos\sqrt{4\pi}\Phi\, L_3R_3. \end{aligned} \tag{24}$$

Here K is a function of the applied magnetic field H as well as the parameter θ. In order to deduce the structure of the ground-state phase diagram of Eq. (24) we may neglect the marginal term $\mathcal{H}_{\rm int}$. This leaves us with a decoupled theory

of an off-critical Ising model $\mathcal{H}_3$ and a sine-Gordon model with a chemical potential equal to the applied magnetic field H. The latter is exactly solvable[64,65] and exhibits two distict phases. If H is less than the critical value $H_{c,1}$ the model remains gapped, while it becomes critical for $H > H_{c,1}$. On the basis of these observations we expect altogether four different phases. The interaction term $\mathcal{H}_{\rm int}$ affects the value of the critical field $H_{c,1}$ and renormalizes the parameters in $\mathcal{H}_3$ and $\mathcal{H}_B$. In addition to the terms written in Eq. (24) further (marginal or irrelevant) interactions will be generated by integrating out high-energy degrees of freedom in the underlying lattice model. In particular, the marginal interaction $\mathcal{H}_{\rm marginal} = \partial_x \Phi R_3 L_3$ appears to be compatible with all symmetries and therefore ought to be generated. While this term is unimportant as long as the Ising model described by $\mathcal{H}_3$ remains off-critical, it could modify the Ising transition itself. The effects of this interaction term have recently been analyzed in the context of a band-filling transition in a two-subband quantum wire by Sitte *et al.*[66] Based on a one-loop renormalization-group calculation it was suggested that $\mathcal{H}_{\rm marginal}$ alters the nature of the quantum phase transition and leads to a scaling behavior that differs from that of $\mathcal{H}_3 + \mathcal{H}_B$ for very large length scales. Due to the nonscalar nature of $\mathcal{H}_{\rm marginal}$ these length scales are expected to be much larger than the system sizes used in our DMRG computations. In the following we therefore will neglect $\mathcal{H}_{\rm marginal}$.

A. Weak magnetic fields $H < H_{c,1}(\theta)$

For weak magnetic fields $H < H_{c,1}(\theta)$ the model (24) is fully gapped. The system remains unmagnetized. There are two phases, which are distinguished by the sign of the mass term in $\mathcal{H}_3$.[63,67] For $\theta - \theta_{TB} > 0$ we have $m > 0$ and the Ising model described by $\mathcal{H}_3$ is in its disordered phase. This corresponds to the Haldane phase. For $\theta - \theta_{TB} < 0$ we have $m < 0$ and the Ising model described by $\mathcal{H}_3$ is in its ordered phase. This corresponds to the dimerized phase.

B. High fields $H > H_{c,1}(\theta)$

When the magnetic field exceeds the critical value $H_{c,1}(\theta)$ the bosonic degrees of freedom described by $\mathcal{H}_B$ enter a gapless Luttinger liquid phase. For $H > H_{c,1}(\theta)$ we end up with an effective Hamiltonian of the form

$$\mathcal{H} = \frac{i\tilde{v}}{2}[L_3\partial_x L_3 - R_3\partial_x R_3] - i\tilde{m}\, R_3 L_3 + \frac{\tilde{v}'}{2}[(\partial_x\tilde{\Phi})^2 + (\partial_x\tilde{\Theta})^2], \tag{25}$$

where the parameters $\tilde{v}$, $\tilde{v}'$, and $\tilde{m}$ depend on the magnetic field H and θ. This can be seen as follows. We may remove the magnetic field term in Eq. (24) by the field redefinitions $\Phi' = \Phi + \frac{K}{v'\sqrt{\pi}} Hx$, $\Theta' = \Theta$. In terms of the new fields the cosine term in $\mathcal{H}_B$ is oscillating in x and for sufficiently large H (compared to m) drops out of the Hamiltonian $\int dx\, \mathcal{H}$ at low energies. Carrying out a unitary rescaling of Φ' and Θ' then leads to Eq. (25) (where we have also taken into account the renormalization of the various parameters in a strong field).

The lattice spin operators are expressed in terms of the new fields as

$$\begin{aligned} S_j^{\pm} &\sim (-1)^j \exp\left(\pm i\frac{\pi}{\beta}\tilde{\Theta}\right)\mu^3 + \cdots, \\ S^z &\sim \cos(\beta\tilde{\Phi} + \pi(1-M)x)\,\sigma^3 + \cdots, \\ (S_j^{\pm})^2 &\sim \exp\left(\pm i\frac{2\pi}{\beta}\tilde{\Theta}\right) + \cdots, \end{aligned} \tag{26}$$

where $\beta > \beta(H_{c,1}) = \sqrt{\pi}$ depends on the applied magnetic field H (Refs. 26 and 50) in a way that cannot be easily calculated from within the field-theory framework. In Eq. (26) we have only written the contributions with the smallest scaling dimensions at the TB point.

The form of Eq. (25) shows that there are two phases separated by an Ising phase transition, which occurs when $\tilde{m}$ is tuned to zero. We are now in a position to describe the behavior of correlation functions in these phases.

1. *Haldane phase in a field*

The case $\tilde{m} > 0$ corresponds to the Haldane phase in a (strong) magnetic field. We note that the closely related case $\theta = 0$, i.e., the spin-1 Heisenberg model in a field, has been discussed previously by several authors; see, e.g., Refs. 50, 51,63 and 68. The Ising model described by L_3, R_3 is in its disordered phase so that

$$\langle\sigma^3\rangle = 0, \qquad \langle\mu^3\rangle \neq 0. \tag{27}$$

More precisely, the expectation value of the Ising disorder operator scales as

$$\langle\mu^3\rangle \propto |\tilde{m}|^{1/8}. \tag{28}$$

If we consider the Ising mass as a function of the parameter θ for fixed magnetic field H, we have very close to the critical point $\theta_c(H)$

$$\tilde{m} \propto |\theta - \theta_c|. \tag{29}$$

Using the expression given in Eq. (26) gives an exponentially decaying contribution to the zz spin correlations. The leading long-distance behavior is therefore due to the terms $\partial_x\tilde{\Phi}$ and $\sin(2\beta\tilde{\Phi} + 2\pi Mx)$,[50,51] which gives

$$C_S^{\rm long}(i,j) \sim \frac{A}{(i-j)^2} + \frac{B\cos[2\pi M(i-j)]}{(i-j)^{2\beta^2/\pi}}. \tag{30}$$

Here the oscillatory contribution is always subleading as $\beta > \sqrt{\pi}$. The dominant correlations are the transverse spin correlations

$$\begin{aligned} C_S^{\rm trans}(i,j) &\sim (-1)^{i-j}\left\langle \exp\left(i\frac{\pi}{\beta}\tilde{\Theta}(x)\right)\exp\left(-i\frac{\pi}{\beta}\tilde{\Theta}(0)\right)\right\rangle \\ &\sim (-1)^{i-j}\,(i-j)^{-\pi/(2\beta^2)}. \end{aligned} \tag{31}$$

Hence we expect a correlation exponent for transverse spin correlations,

$$\frac{\pi}{2\beta^2} < \frac{1}{2}. \tag{32}$$

The high-field phase is an attractive Luttinger liquid with dominant transverse spin correlations, in agreement with

Ref. 50. The long-distance asymptotics of the quadrupolar correlations is

$$C_{Q,2}(i,j) \sim \left\langle \exp\left(i\frac{2\pi}{\beta}\tilde{\Theta}(x)\right)\exp\left(-i\frac{2\pi}{\beta}\tilde{\Theta}(0)\right)\right\rangle \sim (i-j)^{-2\pi/\beta^2}. \quad (33)$$

Hence we have

$$\lim_{|i-j|\to\infty}\frac{\left|C_S^{\rm trans}(i,j)\right|^4}{C_{Q,2}(i,j)} = \text{const} \propto |\theta-\theta_c|, \quad (34)$$

in agreement with the numerical results shown in Fig. 11(a).

In order to make contact with DMRG calculations it is useful to consider Friedel oscillations in S_j^z for a system with boundaries. At the Heisenberg point $\theta = 0$ we may derive the Luttinger liquid description of the magnetized phase of the open chain using a strong-coupling analysis as in Refs. 50 and 51. This results in an effective spin-1/2 Heisenberg XXZ chain with equal boundary magnetic fields on both ends. Standard bosonization methods then give

$$\left\langle S_j^z\right\rangle \sim M + A\frac{\sin(2\pi\tilde{M}j+\pi\varphi)}{\left|\frac{N+1}{\pi}\sin\left(\frac{\pi j}{N+1}\right)\right|^{\beta^2/\pi}}, \quad (35)$$

where N is the length of the chain and

$$\tilde{M} = M + \frac{\frac{1}{2}-M-\varphi}{N+1}. \quad (36)$$

We expect the form of Eq. (35) to hold also away from $\theta = 0$.

2. *Dimerized phase in a field*

Here we have $\tilde{m} < 0$ and the Ising model described by L_3, R_3 is in its ordered phase. Hence we have

$$\langle\sigma^3\rangle \neq 0, \qquad \langle\mu^3\rangle = 0. \quad (37)$$

As a result the contribution to the transverse spin correlations due to the "leading" operator identified in Eq. (26) decay exponentially, as do other contributions we have considered. The asymptotics of the zz spin correlator is

$$C_S^{\rm long}(i,j) \sim (i-j)^{-\beta^2/(2\pi)}\cos\left[\pi(1-M)(i-j)\right] \equiv (i-j)^{-\Delta_1}\cos\left[\pi(1-M)(i-j)\right]. \quad (38)$$

On the other hand, the quadrupolar correlations behave as

$$C_{Q,2}(i,j) \sim (i-j)^{-2\pi/\beta^2} \equiv (i-j)^{-\Delta_2}. \quad (39)$$

Just above $H_{c,1}$ we have $\beta \approx \sqrt{\pi}$, which implies that

$$\Delta_2 \approx 2, \qquad \Delta_1 \approx \tfrac{1}{2}. \quad (40)$$

These agree with the weak-field limit of the Bethe-ansatz analysis above. We furthermore know from the Bethe-ansatz analysis that with increasing field the parameter β grows, which implies that Δ_2 decreases and Δ_1 increases. For sufficiently strong fields the quadrupolar correlations become dominant.

For an open chain we expect Friedel oscillations of the form

$$\left\langle S_j^z\right\rangle \sim M + C\frac{\sin[\pi(1-\tilde{M})j+\pi\varphi']}{\left|\frac{N+1}{\pi}\sin\left(\frac{\pi j}{N+1}\right)\right|^{\beta^2/4\pi}}, \quad (41)$$

where for $M = m/N$ with even m,N we find

$$\tilde{M} = M + \frac{2\varphi' - M}{N+1}. \quad (42)$$

3. *Ising transition*

At the transition we have $\tilde{m} = 0$ and the Ising model is critical. As a result the spin correlators acquire additional power-law factors and become

$$C_s^{\rm trans}(i,j) \sim (-1)^{i-j}\,(i-j)^{-1/4-\pi/(2\beta^2)},$$
$$C_s^{\rm long}(i,j) \sim (i-j)^{-1/4-\beta^2/(2\pi)}\cos\left[\pi(1-M)(i-j)\right],$$
$$C_{Q,2}(i,j) \sim (i-j)^{-2\pi/\beta^2}. \quad (43)$$

Note that this implies that $R(x)$ [Eq. (16)] decays $\sim 1/x$, while comparing expressions (31) and (43) shows that the exponent of the transverse spin correlations jumps upon entering the magnetized Haldane phase by a value of 1/4 independent of the value of the magnetization. In contrast, the exponent of $C_{Q,2}$ changes continuously across the transition. These findings are all in agreement with the numerical results presented in Figs. 4(b), 4(c), and 11.

In conclusion, our combined numerical and field-theoretical analysis supports the picture that the Ising transition identified in the fermionic $S = 3/2$ attractive Hubbard model finds a corresponding counterpart in the pair-unbinding transition of the $S = 1$ BLBQ chain at finite magnetic fields.

VI. SUMMARY AND CONCLUSION

To summarize, by combining extensive DMRG calculations, Bethe ansatz, and field-theoretical arguments we have determined the complete phase diagram of the $S = 1$ BLBQ Heisenberg chain in a magnetic field. At finite magnetizations, it consists of five phases: three single-component LL phases and two two-component LL phases. Two of the single-component LL phases appear when polarizing the system starting from the dimerized phase at negative biquadratic interactions. At large enough fields, the LL realized in this parameter region is a ferroquadrupolar LL, which is connected to a SDW-type of LL at lower fields via a crossover line. In the whole region, the gap to single magnon excitations is finite, and both LL phases are characterized by a quasicondensate of bound pairs of magnons. These two single-channel LLs of pairs of magnons are connected by a continuous transition to the more standard single-component LL phase of single magnons that appears when polarizing the Haldane phase. We determined the transition to belong to the Ising universality class with a central charge of 3/2 due to the contribution of the adjacent LL phases. This transition emerges at the TB point at zero field, showing that the magnetic field moves the universality class from $SU(2)_2$ WZWN at zero field to Luttinger liquid plus Ising at finite fields. The two-component LL phases show up for large positive biquadratic interaction (and positive bilinear interaction). They are separated by a magnetization kink from the magnetized Haldane phase and are characterized by dominant incommensurate correlations of transverse magnetic, respectively quadrupolar, type. It is remarkable that they reflect to a certain extent the behavior at zero field. In particular, the spin-nematic character of the

LL phase identified at zero field in the region $\pi/4 \leqslant \theta \leqslant \pi/2$ survives when applying a magnetic field. It is our hope that this rich phase diagram will further motivate the search for experimental realizations of this model, both in quantum magnetic materials as well as in systems of ultracold atomic gases on optical lattices.

ACKNOWLEDGMENTS

We acknowledge useful discussions with E. Boulat, S. Capponi, K. Penc, J.-D. Picon, J. Sudan, and T.A. Tóth. This work has been supported by the Swiss National Fund and by MaNEP. F.H.L.E. thanks the MPIPKS Dresden for its hospitality and acknowledges funding by EPSRC (Grant No. EP/D050952/1). S.R.M. acknowledges financial support by PIF-NSF (Grant No. 0904017). This research was supported in part by the National Science Foundation under Grant No. NSF PHY05-51164.

APPENDIX A: BETHE ANSATZ ANALYSIS AT THE TAKHTAJAN-BABUJIAN POINT WITH A MAGNETIC FIELD

In this Appendix we describe in more detail the Bethe ansatz analysis of the $S = 1$ BLBQ Heisenberg chain in a magnetic field at the TB point $\theta_{TB} = -\frac{\pi}{4}$. At this point the Hamiltonian takes the form

$$H = \frac{J}{\sqrt{2}} \sum_{j=1}^{L} \mathbf{S}_j \cdot \mathbf{S}_{j+1} - (\mathbf{S}_j \cdot \mathbf{S}_{j+1})^2 - HS^z, \tag{A1}$$

and is known to be solvable by Bethe ansatz[14,69,70] for arbitrary values of the magnetic field H. The ground state is described in terms of the integral equation

$$\rho_2(\lambda) = a_1(\lambda) + a_3(\lambda) - \int_{-A}^{A} d\mu\, [2a_2(\lambda-\mu) + a_4(\lambda-\mu)]\, \rho_2(\mu), \tag{A2}$$

where

$$a_n(\lambda) = \frac{1}{2\pi} \frac{2n}{n^2+\lambda^2}. \tag{A3}$$

The integration boundary A is fixed by the condition

$$\epsilon_2(A) = 0, \tag{A4}$$

where the dressed energy $\epsilon_2(\lambda)$ is a solution of the integral equation

$$\epsilon_2(\lambda) = \epsilon_2^{(0)}(\lambda) - \int_{-A}^{A} d\mu\, [2a_2(\lambda-\mu) + a_4(\lambda-\mu)]\, \epsilon_2(\mu). \tag{A5}$$

Here the "bare energy" is given by

$$\epsilon_2^{(0)}(\lambda) = -\frac{8\pi J}{\sqrt{2}} [a_1(\lambda) + a_3(\lambda)] + 2H. \tag{A6}$$

Ground-state energy and magnetization per site are

$$M = 1 - 2\int_{-A}^{A} d\lambda\, \rho_2(\lambda), \qquad e = \int_{-A}^{A} d\lambda\, \epsilon_2^{(0)}(\lambda)\, \rho_2(\lambda). \tag{A7}$$

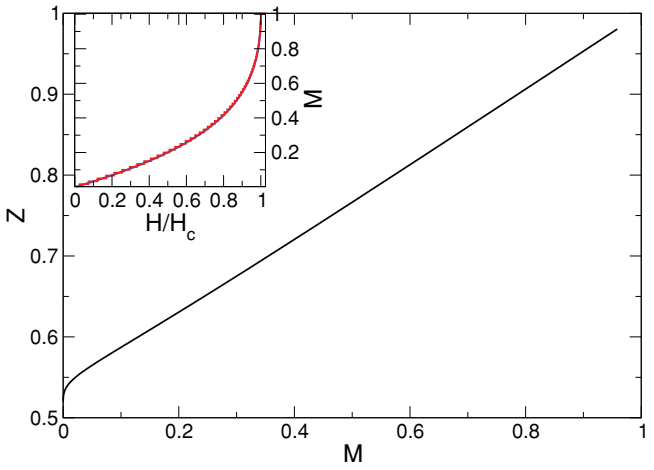

FIG. 12. (Color online) Dressed charge Z as a function of the magnetization per site M as obtained by Bethe ansatz. Inset: magnetization per site M as a function of the applied magnetic field (in units of the saturation field H_c) as obtained by Bethe ansatz (blue straight line) and the DMRG (red steps).

For zero field the determination of the finite-size spectrum of low-lying excitations is difficult because the ground state is made from complex solutions of the Bethe ansatz equations ("2-strings").[71–74] In a finite field matters are simpler and following the standard analysis[75] we can establish that the finite-size spectrum of low-lying excited states is given by

$$\Delta E = \frac{2\pi v}{L} \left[\frac{(\Delta N)^2}{4Z^2} + (Zd)^2 + N^+ + N^- \right], \tag{A8}$$

$$\Delta P = 2k_F d + \frac{2\pi}{L} [N^+ - N^- + d\Delta N]. \tag{A9}$$

Here ΔN and d are integers and the dressed charge $Z = \xi(A)$ is calculated from the integral equation

$$\xi(\lambda) = 1 - \int_{-A}^{A} d\mu\, [2a_2(\lambda-\mu) + a_4(\lambda-\mu)]\, \xi(\mu). \tag{A10}$$

The result is shown in Fig. 12, which depicts the dressed charge Z as a function of the magnetization M. The integer ΔN is related to the z component of the spin by

$$\delta S^z = -2\Delta N. \tag{A11}$$

The "Fermi momentum" k_F is related to the magnetization per site by

$$k_F = \frac{\pi(1-M)}{2}. \tag{A12}$$

The spectrum (A9) describes a Gaussian model, which implies that the asymptotic behavior of correlation functions takes the form[75]

$$\langle \mathcal{O}(t,x)\mathcal{O}^\dagger(0,0)\rangle = \sum_{d,\Delta N, N^\pm} C(d,\Delta N, N^\pm)\, e^{-2ixk_F d} \times (x - ivt)^{-2\Delta^+} (x + ivt)^{-2\Delta^-}, \tag{A13}$$

where

$$2\Delta^{\pm} = 2N^{\pm} + \left(\frac{\Delta N}{2Z} \pm Zd\right)^2. \tag{A14}$$

Which of the amplitudes $C(d,\Delta N,N^{\pm})$ are nonzero depends on the operator under consideration. The smallest correlation exponents for scalar operators are obtained by the choices

$$\begin{aligned} &\Delta N = 0, \quad d = 1 \longrightarrow \Delta_1 = 2Z^2, \\ &d = 0, \quad \Delta N = 1 \longrightarrow \Delta_2 = \frac{1}{2Z^2}. \end{aligned} \tag{A15}$$

The z component of the spin S^z_j is sensitive only to states with $\Delta N = 0$, while $(S^-_j)^2$ changes the total spin by 2 and hence couples to states with $\Delta N = 1$. This analysis then suggests that the leading long-distance behavior of correlation functions is of the form

$$\begin{aligned} &C_S^{\text{long}}(i,j) \sim (i-j)^{-\Delta_1}\cos[\pi(1-M)(i-j)], \\ &C_{Q,2}(i,j) \sim (i-j)^{-\Delta_2}, \end{aligned} \tag{A16}$$

The exponents $\Delta_{1,2}$ are shown as functions of the applied magnetic field in Fig. 5. We see that for weak fields the longitudinal spin correlations dominate, while for strong fields the quadrupolar correlations decay more slowly. The crossover occurs at a magnetization per site of $M_c \approx 0.37$.

APPENDIX B: BETHE ANSATZ SOLUTION FOR $\theta = \theta_{ULS} = \frac{\pi}{4}$

Here we describe in more detail the Bethe ansatz analysis of the SU(3) Uimin-Lai-Sutherland model[11–13] in a magnetic field, which corresponds to the point $\theta_{ULS} = \frac{\pi}{4}$. For this value of θ the Hamiltonian takes the form

$$H = \frac{J}{\sqrt{2}}\sum_{j=1}^{L} \mathbf{S}_j \cdot \mathbf{S}_{j+1} + (\mathbf{S}_j \cdot \mathbf{S}_{j+1})^2 - hS^z, \tag{B1}$$

and is known to be solvable by Bethe ansatz for arbitrary values of the magnetic field H. The critical properties of the model have been previously analyzed in Ref. 31 and we begin by summarizing the results obtained there.

1. Ground-state properties

The ground state is described in terms of the coupled integral equations

$$\rho_a(\lambda) = \rho_a^{(0)}(\lambda) + \sum_{b=1}^{2}\int_{-A_b}^{A_b} d\mu K_{ab}(\lambda-\mu)\rho_b(\mu), \tag{B2}$$

where

$$K_{12}(\lambda) = K_{21}(\lambda) = a_1(\lambda), \tag{B3}$$

$$K_{11}(\lambda) = K_{22}(\lambda) = -a_2(\lambda), \tag{B4}$$

$$\rho_a^{(0)}(\lambda) = -2\pi\delta_{a1}a_1(\lambda), \tag{B5}$$

with $a_n(\lambda)$ defined in Eq. (A3). By virtue of the enhanced SU(3) symmetry of the model (B1) in zero field the numbers M_σ of σ spins ($\sigma = 1,0,-1$) are good quantum numbers. The z component of total spin is one of the Cartan generators of SU(3) and hence M_σ remain good quantum numbers even in the presence of a magnetic field. By definition we have $L = M_1 + M_0 + M_{-1}$ and in the ground state we have

$$n_1 = \frac{N_1}{L} = \frac{M_0 + M_{-1}}{L} = \int_{-A_1}^{A_1} d\lambda\rho_1(\lambda), \tag{B6}$$

$$n_2 = \frac{N_2}{L} = \frac{M_{-1}}{L} = \int_{-A_2}^{A_2} d\lambda\rho_2(\lambda). \tag{B7}$$

The conditions (B7) fix the integration boundaries $A_{1,2}$ as functions of the densities $n_{1,2}$. The magnetization per site is

$$\begin{aligned} M &= \frac{M_1 - M_{-1}}{L} = 1 - \sum_{b=1}^{2}\int_{-A_b}^{A_b} d\lambda\ \rho_b(\lambda) \\ &= 1 - n_1 - n_2. \end{aligned} \tag{B8}$$

The integration boundaries $A_{1,2}$ are determined by the applied magnetic field through the conditions

$$\epsilon_b(A_b) = 0, \tag{B9}$$

where the dressed energies $\epsilon_b(\lambda)$ are solutions of the coupled integral equations

$$\epsilon_a(\lambda) = \epsilon_a^{(0)}(\lambda) + \sum_{b=1}^{2}\int_{-A_b}^{A_b} d\mu K_{ab}(\lambda-\mu)\epsilon_b(\mu). \tag{B10}$$

Here the "bare energies" are given by

$$\epsilon_1^{(0)}(\lambda) = -2\pi a_1(\lambda) + h, \tag{B11}$$

$$\epsilon_2^{(0)}(\lambda) = h. \tag{B12}$$

As a function of magnetic field there are four distinct regimes:

(1) $h = 0$: as a result of the enhanced symmetry the low-energy physics is described by the $SU_1(3)$ WZNW model. The central charge is $c = 2$.

(2) $0 < h < h_{c,1}$: the model remains in a quantum critical phase. Universal properties are described by a two-component Luttinger liquid. The central charge is $c = 2$, but the symmetry is reduced as compared to $h = 0$. When h approaches $h_{c,1}$ the cutoff of one of the Luttinger liquids goes to zero.

(3) $h_{c,1} < h < h_{c,2}$: the low-energy physics is described by a $c = 1$ one-component Luttinger liquid.

(4) $h_{c,2} < h$: the ground state is fully polarized and all excitations have a gap.

In the following we concentrate on the two-component Luttinger liquid regime $0 < h < h_{c,1}$. In Fig. 13 we plot the magnetization per site as a function of the applied magnetic field and the densities $n_{1,2}$ as functions of the magnetization. We see that at $h_{c,1}$ the density of $S^z = -1$ spins becomes zero.

2. Low-lying excitations for $0 < h < h_{c,1}$

As we are dealing with a quantum critical theory there are gapless excitations. In a finite volume L the spectrum of low-lying excited states scales as L^{-1} and is related to the operator content of the underlying conformal field theory.[76] The finite-size energies and momenta of low-lying excitations

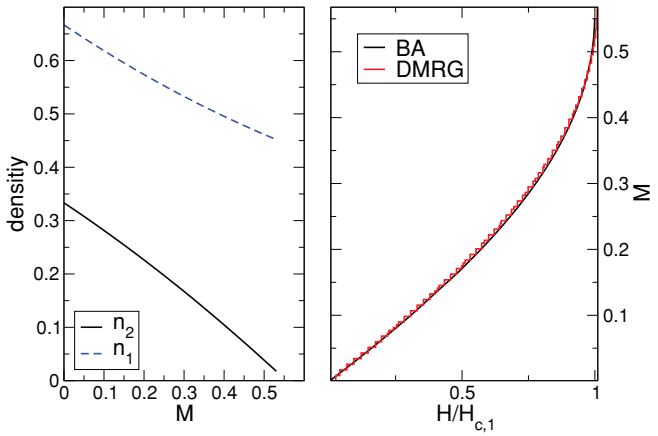

FIG. 13. (Color online) Densities $n_{1,2}$ as functions of the magnetization per site as obtained by Bethe ansatz and magnetization per site as a function of the applied magnetic field as obtained by Bethe ansatz (black straight line) and DMRG (red steps).

can be determined by standard methods[77–79] from the Bethe ansatz solution with the result[31]

$$E(\Delta\mathbf{N},\mathbf{d}) - E_0 = \frac{2\pi}{L}\sum_{a=1}^{2} v_a(\Delta_a^+ + \Delta_a^-) + o\left(\frac{1}{L}\right),$$

$$P(\Delta\mathbf{N},\mathbf{d}) - P_0 = \frac{2\pi}{L}\sum_{a=1}^{2}\Delta_a^+ - \Delta_a^- + 2\pi(n_1 d_1 + n_2 d_2) + \pi\Delta N_1, \tag{B13}$$

where the conformal dimensions $\Delta_{1,2}^{\pm}$ are expressed as

$$\Delta_1^{\pm}(\Delta\mathbf{N},\mathbf{d},N_1^{\pm}) = \frac{1}{2}\left(Z_{11}d_1 + Z_{21}d_2 \pm \frac{Z_{22}\Delta N_1 - Z_{12}\Delta N_2}{2\det Z}\right)^2 + N_1^{\pm}, \tag{B14}$$

$$\Delta_2^{\pm}(\Delta\mathbf{N},\mathbf{d},N_2^{\pm}) = \frac{1}{2}\left(Z_{12}d_1 + Z_{22}d_2 \pm \frac{Z_{11}\Delta N_2 - Z_{21}\Delta N_1}{2\det Z}\right)^2 + N_2^{\pm}.$$

Here $N_a^{\pm}$ and $\Delta N_{1,2}$ are integer numbers,

$$d_1 = \frac{\Delta N_2}{2} \bmod 1, \qquad d_2 = \frac{\Delta N_1}{2} \bmod 1, \tag{B15}$$

and $v_{1,2}$ are Fermi velocities of the two types of elementary excitations. They are given in terms of the integral equations (B10), (B2) by

$$v_a = \frac{\epsilon_a'(A_a)}{2\pi\rho_a(A_a)}, \tag{B16}$$

where $\epsilon_a'(\lambda)$ are the derivatives of the dressed energies. Finally, Z_{ab} are the elements of the *dressed charge matrix*

$$Z = \begin{pmatrix} \xi_{1c}(A_1) & \xi_{12}(A_2) \\ \xi_{21}(A_1) & \xi_{22}(A_2) \end{pmatrix}, \tag{B17}$$

where ξ_{ab} fulfill the set of coupled integral equations

$$\xi_{ab}(\lambda) = \delta_{ab} + \sum_{c=1}^{2}\int_{-A_c}^{A_c} d\mu\ \xi_{ac}(\mu)\ K_{cb}(\mu - \lambda). \tag{B18}$$

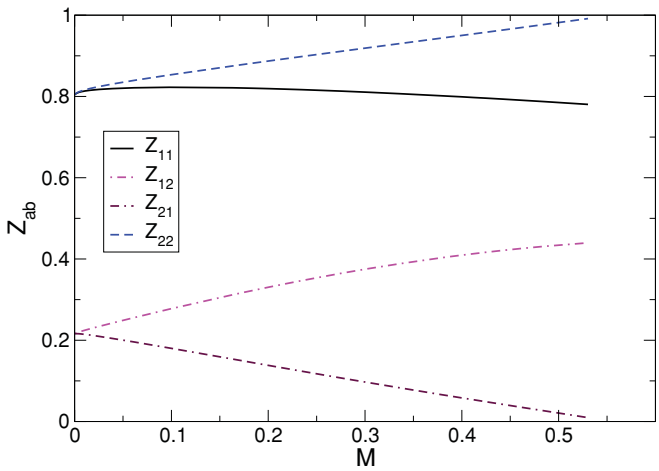

FIG. 14. (Color online) Elements of the dressed charge matrix Z as functions of the magnetization per site M as obtained by Bethe ansatz.

In Fig. 14 we plot the elements of the dressed charge matrix Z as functions of the magnetization.

3. Long-distance asymptotics of correlation functions

As the critical behavior is described by a two-component Luttinger liquid the asymptotic behavior of correlation functions can be extracted from the finite-size spectrum following the analysis of Frahm and Korepin for the Hubbard model.[79,80] The asymptotic behavior of the two-point function of a local operator $\mathcal{O}$ is given by

$$\langle\mathcal{O}(x)\mathcal{O}^\dagger(0)\rangle = \sum_{\mathbf{d},\Delta\mathbf{N},\mathbf{N}^\pm} C(\mathbf{d},\Delta\mathbf{N},\mathbf{N}^\pm)\, x^{-\Delta} \times e^{-2\pi i(n_1 d_1 + n_2 d_2 + (1/2)\Delta N_1)}, \tag{B19}$$

where the exponents Δ are related to the finite-size energies by

$$\Delta(\mathbf{d},\Delta\mathbf{N},\mathbf{N}^+,\mathbf{N}^-) = 2\Delta_1^+ + 2\Delta_1^- + 2\Delta_2^+ + 2\Delta_2^-. \tag{B20}$$

For a given operator $\mathcal{O}$ certain amplitudes $C(d,\Delta N,N^\pm)$ will be zero due to continuous or discrete symmetries, which sometimes are not entirely obvious.[81] For later use we define a number of momenta characterizing the oscillatory behavior of correlation functions

$$\begin{aligned} P_1 &= 2\pi(n_1 - n_2), \\ P_2 &= \pi(1 - n_2), \\ P_3 &= \pi(1 + n_1 - n_2). \end{aligned} \tag{B21}$$

4. Longitudinal spin correlations

As S_j^z does not change the total z component of spin only intermediate states for which $S^z = L - N_1 - N_2$ is the same as in the ground state will contribute to the correlation function. Hence the longitudinal correlations are characterized by quantum numbers subject to the selection rule

$$\Delta N_1 + \Delta N_2 = 0. \tag{B22}$$

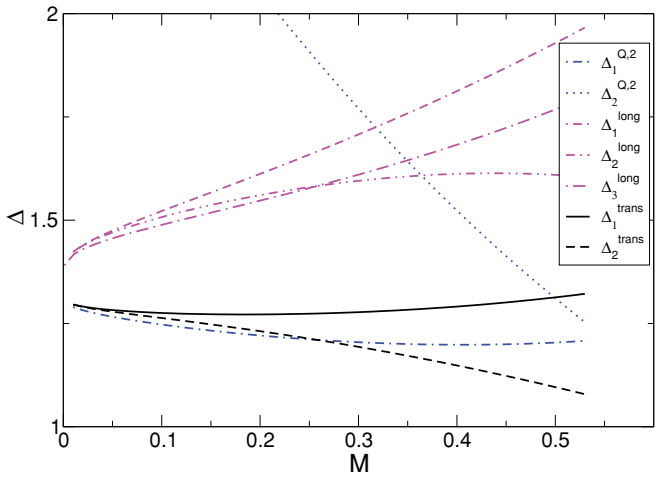

FIG. 15. (Color online) Exponents characterizing the power-law decays of the various correlators as functions of the magnetization per site.

The smallest exponents are then obtained by the following choices:

(1) $\Delta N_{1,2} = 0, \quad d_1 = \pm 1, d_2 = 0, N^{\pm} = 0,$
(2) $\Delta N_{1,2} = 0, \quad d_1 = 0, d_2 = \pm 1, N^{\pm} = 0,$
(3) $\Delta N_{1,2} = 0, \quad d_1 = -d_2 = \pm 1, N^{\pm} = 0,$
(4) $\Delta N_{1,2} = 0, \quad d_1 = d_2 = 0, N^{-} = 0, N^{+} = 1,$
(5) $\Delta N_{1,2} = 0, \quad d_1 = d_2 = 0, N^{-} = 1, N^{+} = 0.$

This leads to the following form for $C_S^{\text{long}}(i,j)$:

$$\begin{aligned} C_S^{\text{long}}(i,j) \sim\ & C_1(i-j)^{-\Delta_1^{\text{long}}} \cos\left[2\pi n_1 (i-j)\right] \\ & + C_2(i-j)^{-\Delta_2^{\text{long}}} \cos\left[2\pi n_2 (i-j)\right] \\ & + C_3(i-j)^{-\Delta_3^{\text{long}}} \cos\left[P_1 (i-j)\right] \\ & + C_4(i-j)^{-2} + \cdots, \end{aligned} \tag{B23}$$

where

$$\begin{aligned} \Delta_1^{\text{long}} &= 2\left(Z_{11}^2 + Z_{12}^2\right), \\ \Delta_2^{\text{long}} &= 2\left(Z_{21}^2 + Z_{22}^2\right), \\ \Delta_3^{\text{long}} &= 2(Z_{11} - Z_{21})^2 + 2(Z_{12} - Z_{22})^2. \end{aligned} \tag{B24}$$

The magnetization dependence of $\Delta_{1,2,3}^{\text{long}}$ is shown in Fig. 15.

5. Transverse spin correlations

In the transverse spin correlator only intermediate states with

$$\Delta N_1 + \Delta N_2 = \pm 1 \tag{B25}$$

contribute. The smallest exponents are then obtained by the following choices:

(1) $\Delta N_1 = \pm 1, \quad d_2 = \pm \frac{1}{2}, \quad \Delta N_2 = d_1 = N^{\pm} = 0,$
(2) $\Delta N_2 = \pm 1, \quad d_1 = \pm \frac{1}{2}, \quad \Delta N_1 = d_2 = N^{\pm} = 0.$

This leads to the following form for $C_S^{\text{trans}}(i,j)$:

$$\begin{aligned} C_S^{\text{trans}}(i,j) \sim\ & D_1(i-j)^{-\Delta_1^{\text{trans}}} \cos\left[P_2 (i-j)\right] \\ & + D_2(i-j)^{-\Delta_2^{\text{trans}}} \cos\left[\pi n_1 (i-j)\right] \\ & + \cdots, \end{aligned} \tag{B26}$$

where the exponents are given by

$$\begin{aligned} \Delta_1^{\text{trans}} &= \left[Z_{21}^2 + Z_{22}^2\right] \frac{1 + \det^2 Z}{2 \det^2 Z}, \\ \Delta_2^{\text{trans}} &= \left[Z_{12}^2 + Z_{11}^2\right] \frac{1 + \det^2 Z}{2 \det^2 Z}. \end{aligned} \tag{B27}$$

The magnetization dependence of $\Delta_{1,2}^{\text{trans}}$ is shown in Fig. 15. We see that the two exponents are comparable in magnitude but $\Delta_2^{\text{trans}} < \Delta_1^{\text{trans}}$.

6. Quadrupolar correlations

Here the operator $\mathcal{O}$ in Eq. (B19) changes the z component of total spin by ± 2, so that we need to consider intermediate states with $\Delta N_1 + \Delta N_2 = \pm 2$. The smallest exponents are then obtained by the following choices:

(1) $\Delta N_1 = \Delta N_2 = \pm 1, \quad d_1 = -d_2 = \pm \frac{1}{2}, \quad N^{\pm} = 0,$
(2) $\Delta N_2 = 2, \quad \Delta N_1 = d_{1,2} = N^{\pm} = 0.$

This leads to the following form for $C_Q(i,j)$:

$$\begin{aligned} C_{Q,2}(i,j) \sim\ & E_1(i-j)^{-\Delta_{Q,2}^{(1)}} \cos\left[P_3 (i-j)\right] \\ & + E_2(i-j)^{-\Delta_{Q,2}^{(2)}} \\ & + \cdots, \end{aligned} \tag{B28}$$

where the exponents are given by

$$\begin{aligned} \Delta_1^{Q,2} &= \left[(Z_{11} - Z_{21})^2 + (Z_{12} - Z_{22})^2\right] \frac{1 + \det^2 Z}{2 \det^2 Z}, \\ \Delta_2^{Q,2} &= 2 \frac{Z_{11}^2 + Z_{21}^2}{\det^2 Z}. \end{aligned} \tag{B29}$$

The magnetization dependence of $\Delta_{1,2}^{Q,2}$ is shown in Fig. 15.

a. Dominant power-law correlations

We are now in a position to identify the dominant power-law correlations. In Fig. 7 we plot the magnetization dependence of the smallest exponents. We see that at low magnetizations the quadrupolar correlation dominates, while for larger magnetizations the transverse spin correlations are seen to decay slowest. The crossover between these two regimes occurs at $M \approx 0.258$.

*Present address: JILA (University of Colorado and NIST), and Department of Physics, CU Boulder, CO 80309-0440, USA.

[1] A. F. Andreev and I. A. Grishchuk, Sov. Phys. JETP **60**, 267 (1984).
[2] A. Chubukov, J. Phys.: Condens. Matter **2**, 1593 (1990).
[3] S. Nakatsuji, Y. Nambu, H. Tonomura, O. Sakai, S. Jonas, C. Broholm, H. Tsunetsugu, Y. Qiu, and Y. Maeno, Science **309**, 1697 (2005).

[4] A. Läuchli, F. Mila, and K. Penc, Phys. Rev. Lett. **97**, 087205 (2006).

[5] H. Tsunetsugu and M. Arikawa, J. Phys. Soc. Jpn. **75**, 083701 (2006).

[6] *Quantum Magnetism*, *Lecture Notes in Physics*, by U. Schollwöck, J. Richter, D. J. J. Farnell, and R. F. Bishop (Springer-Verlag, Berlin/Heidelberg, 2004).

[7] F. Mila and F.-C. Zhang, Eur. Phys. J. B **16**, 7 (2000).

[8] J. J. García-Ripoll, M. A. Martin-Delgado, and J. I. Cirac, Phys. Rev. Lett. **93**, 250405 (2004).

[9] S. Trotzky, P. Cheinet, S. Folling, M. Feld, U. Schnorrberger, A. M. Rey, A. Polkovnikov, E. A. Demler, M. D. Lukin, and I. Bloch, Science **319**, 295 (2008).

[10] A. V. Gorshkov, M. Hermele, V. Gurarie, C. Xu, P. S. Julienne, J. Ye, P. Zoller, E. Demler, M. D. Lukin, and A. M. Rey, Nat. Phys. **6**, 289 (2010).

[11] G. V. Uimin, JETP Lett. **12**, 225 (1970).

[12] C. K. Lai, J. Math. Phys. **15**, 1675 (1974).

[13] B. Sutherland, Phys. Rev. B **12**, 3795 (1975).

[14] L. Takhtajan, Phys. Lett. A **87**, 479 (1982).

[15] H. Babujian, Phys. Lett. A **90**, 479 (1982).

[16] I. Affleck, T. Kennedy, E. H. Lieb, and H. Tasaki, Phys. Rev. Lett. **59**, 799 (1987).

[17] M. N. Barber and M. T. Batchelor, Phys. Rev. B **40**, 4621 (1989).

[18] A. Klümper, Europhys. Lett. **9**, 815 (1989).

[19] Y. Xian, Phys. Lett. A **183**, 437 (1993).

[20] G. Fáth and J. Sólyom, Phys. Rev. B **44**, 11836 (1991).

[21] G. Fáth and J. Sólyom, Phys. Rev. B **47**, 872 (1993).

[22] U. Schollwöck, T. Jolicœur, and T. Garel, Phys. Rev. B **53**, 3304 (1996).

[23] K. Buchta, G. Fáth, O. Legeza, and J. Sólyom, Phys. Rev. B **72**, 054433 (2005).

[24] A. Läuchli, G. Schmid, and S. Trebst, Phys. Rev. B **74**, 144426 (2006).

[25] F. D. M. Haldane, Phys. Lett. A **93**, 464 (1983).

[26] F. D. M. Haldane, Phys. Rev. Lett. **50**, 1153 (1983).

[27] G. Fáth and A. Sütő, Phys. Rev. B **62**, 3778 (2000).

[28] J. Parkinson, J. Phys.: Condens. Matter **1**, 6709 (1989).

[29] K. Okunishi, Y. Hieida, and Y. Akutsu, Phys. Rev. B **60**, 6953(R) (1999).

[30] K. Okunishi, Y. Hieida, and Y. Akutsu, Phys. Rev. B **59**, 6806 (1999).

[31] G. Fáth and P. B. Littlewood, Phys. Rev. B **58**, 14709(R) (1998).

[32] S. R. White, Phys. Rev. Lett. **69**, 2863 (1992).

[33] U. Schollwöck, Rev. Mod. Phys. **77**, 259 (2005).

[34] A. Kolezhuk and T. Vekua, Phys. Rev. B **72**, 094424 (2005).

[35] K. Harada and N. Kawashima, Phys. Rev. B **65**, 052403 (2002).

[36] P. Corboz, A. M. Läuchli, K. Totsuka, and H. Tsunetsugu, Phys. Rev. B **76**, 220404 (2007).

[37] T. Vekua, A. Honecker, H.-J. Mikeska, and F. Heidrich-Meisner, Phys. Rev. B **76**, 174420 (2007).

[38] L. Kecke, T. Momoi, and A. Furusaki, Phys. Rev. B **76**, 060407 (2007).

[39] T. Hikihara, L. Kecke, T. Momoi, and A. Furusaki, Phys. Rev. B **78**, 144404 (2008).

[40] J. Sudan, A. Lüscher, and A. M. Läuchli, Phys. Rev. B **80**, 140402 (2009).

[41] I. P. McCulloch, R. Kube, M. Kurz, A. Kleine, U. Schollwöck, and A. K. Kolezhuk, Phys. Rev. B **77**, 094404 (2008).

[42] M. Henkel, *Conformal Invariance and Critical Phenomena* (Springer, Berlin, 1999).

[43] Ö. Legeza, J. Sólyom, L. Tincani, and R. M. Noack, Phys. Rev. Lett. **99**, 087203 (2007).

[44] P. Calabrese and J. Cardy, J. Stat. Mech.: Theory Exp. **2004**, P06002 (2004).

[45] F. Heidrich-Meisner, A. Honecker, and T. Vekua, Phys. Rev. B **74**, 020403 (2006).

[46] A. V. Chubukov, Phys. Rev. B **44**, 4693 (1991).

[47] F. Heidrich-Meisner, I. P. McCulloch, and A. K. Kolezhuk, Phys. Rev. B **80**, 144417 (2009).

[48] K. P. Schmidt, J. Dorier, A. Läuchli, and F. Mila, Phys. Rev. B **74**, 174508 (2006).

[49] G. Fáth, Phys. Rev. B **68**, 134445 (2003).

[50] R. M. Konik and P. Fendley, Phys. Rev. B **66**, 144416 (2002).

[51] A. Furusaki and S.-C. Zhang, Phys. Rev. B **60**, 1175 (1999).

[52] L. Campos Venuti, E. Ercolessi, G. Morandi, P. Pieri, and M. Roncaglia, Int. J. Mod. Phys. B **16**, 1363 (2002).

[53] A. Friedrich, A. K. Kolezhuk, I. P. McCulloch, and U. Schollwöck, Phys. Rev. B **75**, 094414 (2007).

[54] K. Penc (private communication).

[55] A. M. Tsvelik, *Quantum Field Theory in Condensed Matter Physics* (Cambridge University Press, Cambridge, England, 2003).

[56] S. Ejima, M. J. Bhaseen, M. Hohenadler, F. H. L. Essler, H. Fehske, and B. D. Simons, Phys. Rev. Lett. **106**, 015303 (2011).

[57] P. Lecheminant, E. Boulat, and P. Azaria, Phys. Rev. Lett. **95**, 240402 (2005).

[58] C. Wu, Phys. Rev. Lett. **95**, 266404 (2005).

[59] P. Lecheminat, E. Boulat, and P. Azaria, Nucl. Phys. B **798**, 443 (2008).

[60] S. Capponi, G. Roux, P. Azaria, E. Boulat, and P. Lecheminant, Phys. Rev. B **75**, 100503(R) (2007).

[61] G. Roux, S. Capponi, P. Lecheminant, and P. Azaria, Eur. Phys. J. B **68**, 293 (2009).

[62] L. Bonnes and S. Wessel, Phys. Rev. Lett. **106**, 185302 (2011).

[63] A. M. Tsvelik, Phys. Rev. B **42**, 10499 (1990).

[64] F. Haldane, J. Phys. A **15**, 507 (1982).

[65] J.-S. Caux and A. Tsvelik, Nucl. Phys. B **474**, 715 (1996).

[66] M. Sitte, A. Rosch, J. S. Meyer, K. A. Matveev, and M. Garst, Phys. Rev. Lett. **102**, 176404 (2009).

[67] A. A. Nersesyan and A. M. Tsvelik, Phys. Rev. Lett. **78**, 3939 (1997).

[68] I. Affleck, Phys. Rev. B **43**, 3215 (1991).

[69] H. Babujian, Nucl. Phys. B **215**, 317 (1983).

[70] A. Tsvelik, Nucl. Phys. B **305**, 675 (1988).

[71] F. Alcaraz and M. Martins, J. Phys. A **22**, 1829 (1989).

[72] F. Alcaraz and M. Martins, J. Phys. A **23**, 1439 (1990).

[73] H. Frahm and N.-C. Yu, J. Phys. A **23**, 2115 (1990).

[74] H. Frahm, N.-C. Yu, and M. Fowler, Nucl. Phys. B **336**, 396 (1990).

[75] V. Korepin, A. Izergin, and N. Bogoliubov, *Quantum Inverse Scattering Method, Correlation Functions and Algebraic Bethe Ansatz* (Cambridge University Press, Cambridge, England, 1993).

[76] J. L. Cardy, Nucl. Phys. B **270**, 186 (1986).

[77] F. Woynarovich, J. Phys. A **22**, 4243 (1989).

[78] H. Frahm and V. E. Korepin, Phys. Rev. B **42**, 10553 (1990).

[79] F. H. L. Essler, H. Frahm, F. Göhmann, A. Klümper, and V. E. Korepin, *The One-Dimensional Hubbard Model* (Cambridge University Press, Cambridge, England, 2005).

[80] H. Frahm and V. E. Korepin, Phys. Rev. B **43**, 5653 (1991).

[81] F. H. L. Essler and H. Frahm, Phys. Rev. B **60**, 8540 (1999).